Lipid Specificity of the Fusion of Bacterial Extracellular Vesicles with the Host Membrane

Ashutosh Prince[1,2#], Anuj Tiwari[1†], Titas Mandal[3†], Debraj Koiri[5,6], Geetanjali Meher[5,6], Deepak Kumar Sinha[4], Mohammed Saleem[5,6]*

[1]Department of Life Sciences, National Institute of Technology, Rourkela, India.

[2]Center for Gene Regulation in Health and Disease, Cleveland State University, Cleveland, OH, United States.

[3]Department of Physical Biochemistry, University of Potsdam, Germany.

[4]Department of Biological Chemistry, Indian Association for the Cultivation of Sciences, Kolkata, India.

[5]School of Biological Sciences, National Institute of Science Education and Research, Bhubaneswar, India.

[6]Homi Bhabha National Institute, Mumbai, India.

[#] Current Affiliation

† Equal Contribution

* Corresponding author: Mohammed Saleem.

Email: saleem@niser.ac.in

Contact: +91-674-2494501

Keywords

Bacterial membrane vesicles; Membrane reconstitution; Fluorescence anisotropy; Dipole potential; Compressibility modulus.

Abstract

Bacterial membrane vesicles (MVs) facilitate long-distance delivery of virulence factors crucial for pathogenicity. The entry and trafficking mechanisms of virulence factors inside host cells are recently emerging, however, if bacterial MVs can fuse and modulate the physicochemical properties of the host lipid membrane and membrane lipid parameter for fusion remains unknown. Here we reconstitute the interaction of bacterial MV with host cell lipid membranes and quantitatively show that bacterial MV interaction increases the fluidity, dipole potential, and Compressibility of a biologically relevant multi-component host membrane upon fusion. The presence of cylindrical lipids such as phosphatidylcholine and a moderate acyl chain length of C16 helps the MV interaction. While significant binding of bacterial MVs to the raft-like lipid membranes with phase-separated regions of the membrane was observed, however, MVs prefer binding to the liquid-disordered regions of the membrane. Further, the elevated levels of cholesterol tend to hinder the interaction of bacterial MVs as evident from the favorable excess Gibbs free energy of mixing of bacterial MVs with host lipid membranes. The findings provide new insights that might have implications for the regulation of host machinery by bacterial pathogens through the manipulation of host membrane properties.

Introduction

The secretion of membrane vesicles (MVs) from the bacterial cells is recognized as a generalized phenomenon observed in many bacteria [1]. Bacterial MVs are known to facilitate contact-free inter-species communication, nutrient acquisition, enhanced survival against immune response and host-pathogen interaction [2]. Initially known to be only secreted by controlled blebbing of Gram negative bacteria, emerging evidence supports the existence of different types of Bacterial MV, such as – Bacterial extracellular vesicles (MVs), Outer-inner membrane vesicles (OIBMVs) and Explosive outer membrane vesicles (EOBMVs) all of which are involved in transport of virulence factors [3]. Typically, bacterial MVs are nano-sized spherical membrane compartments spanning 20-300 nm in diameter derived from the outer membrane lipid bilayer and the periplasm of the bacteria [2]. Biochemically, bacterial MVs are known to carry lipopolysaccharides (LPS), phospholipids, peptidoglycans, outer membrane proteins (OMPs), nucleic acids, signaling

56 molecules and periplasmic, cytoplasmic and membrane-bound proteins [4]. The degree of
57 bacterial MV secretion has also been correlated to the pathogenicity and virulence of
58 bacteria [5]. Interestingly, in addition to delivering a selection of virulence factors and
59 immunomodulatory molecules directly into host cells during infection, bacterial MVs are
60 also known to act as decoy antigen and divert the host immune system away from the
61 bacterial cell [6]. There is a considerable focus on the understanding of the virulence factors
62 of the MV cargo and modes of bacterial MV entry inside host cells. Owing to a wide range
63 of size of bacterial MVs, different pathways such as macropinocytosis, clathrin-dependent
64 and caveolin or lipid raft mediated endocytosis have been implicated in the internalization
65 processes of different Bacterial MVs [7]. Further, direct membrane fusion with host cell
66 membranes, preferentially at lipid raft domains, has also been reported to be a potential
67 mechanism of entry of bacterial MVs [8]. Similarly, fusion of bacterial MVs extracted from
68 *L. pneumophila* with host model membranes suggested the faster time scales of fusion
69 events (few seconds), which is also temperature-dependent [9].

70 A crucial aspect that remains unexplored is if/how MV fusion modulates the
71 physicochemical parameters of host cell membranes (i.e., fluidity, dipole potential and in-
72 plane Compressibility). Irrespective of the kind of bacterial MVs, mode of entry of
73 bacterial MVs, insights on membrane interfacial interaction of bacterial MVs is crucial as
74 the local lipid reorganization and remodeling of the host cell membrane is a prerequisite
75 for MV entry. It is proposed that the MV fusion may result in changes in the properties of
76 the host cell membrane [9], however, there is no experimental evidence in support of this
77 idea. The lipid specificity, quantitative changes in physicochemical parameters (e.g.,
78 fluidity, dipole potential and in-plane Compressibility) of host membrane triggered by
79 bacterial MVs and the thermodynamics of their interaction has never been explored to best
80 of our knowledge.

81 Using *in vitro* reconstitution, confocal laser scanning microscopy, potentiometric dye-
82 based fluorescence anisotropy, dipole potential measurements and surface pressure-area
83 isotherms, we show that MV interaction increases the fluidity, dipole potential and in-plane
84 Compressibility of the lipid membranes mimicking the host cell membrane. We also report
85 the role of host membrane lipid head-group specificity, acyl chain length and phase

separated boundaries on the interfacial interaction of bacterial MVs. The presence of lipids such as 1,2-dioleoyl-*sn*-glycero-3-phosphocholine (DOPC) and an acyl chain length of C16 are significant for the fusion of the bacterial MVs. Furthermore, the bacterial MVs prefer liquid disordered regions of the lipid membrane, whereas the elevated levels of cholesterol in raft-like lipid membranes with phase separated regions tend to hinder the interaction. The findings are further supported by the investigation of the thermodynamic parameters of MV interaction with host lipid membrane, revealing the change in Gibbs excess free energy of mixing of MV components with biologically relevant host membrane lipid membrane conditions. These findings show that bacterial membrane vesicles can effectively modulate the physicochemical properties of the host membrane that might eventually have consequences for membrane associated signaling during host-pathogen interactions.

Materials and Methods

Materials

Calcium chloride ($CaCl_2$), HEPES, sodium chloride (NaCl), TX-100, Lauria Bertini (LB) broth, methanol, chloroform, Nile red were purchased from Himedia, India. Di-8-ANEPPS, Vybrant DiO were procured from ThermoFisher, USA. N-ethylmaleimide (NEM), Dimethylsulphoxide (DMSO) and RPMI media were purchased from Sigma Aldrich, USA. All lipids used in study, 1,2-dioleoyl-*sn*-glycero-3-phosphocholine (DOPC), 1,2-dilauroyl-sn-glycero-3-phosphocholine (DLPC), 1,2-dimyrisitol-sn-glycero-3-phophocholine (DMPC), 1,2-distearoyl-sn-glycero-3-phosphocholine (DSPC), 1,2-dipalmitoyl-sn-glycero-3-phosphocholine (DPPC), Sphingomyelin from Brain Porcine (BSM), cholesterol, 1,2-dioleoyl-sn-glycero-3-phosphoethanolamine (DOPE), 1,2-dioleoyl-sn-glycero-3-phophoethanolamine-N-(7-nitro-2-1,3-benzoxadiazol-4-yl) (NBD-PE), 1,2-dipalmitoyl-sn-glycero-3-phosphoethanolamine-N-(lissamine rhodamine B sulfonyl (Rhodamine-PE) were purchased from Avanti Polar lipids, USA. Monocytic leukemia cell lines (THP-1) were purchased from the National Center of Cell Science, Pune, India. *E. coli* used for isolation of extracellular vesicles was procured from Institute of Microbial Technology, Chandigarh, India.

116 ## Preparation of Buffers and Solutions

117 Membrane vesicle (MV) buffer containing 10 mM HEPES, 2 mM $CaCl_2$ and 150 mM NaCl
118 prepared in deionized water with physiological pH of 7.4. 3mM N-ethylmaleimide (NEM)
119 solution was made freshly during the experiment by dissolving NEM in miliQ water. Nile
120 red powder was dissolved in DMSO (dimethylsulphoxide) to the final concentration of 100
121 nM. DiO labelling stock solution was prepared by dissolving 1mg DiO in 1 mL of DMSO.

122 ## Membrane Vesicles Purification from Bacteria

123 *E. coli* were used for the vesiculation and isolation of bacterial membrane vesicles (MVs).
124 The methodology for MV vesiculation and isolation was adopted from the procedure
125 described by Sezgin et. al. [10] with some modification and optimization that allowed us to
126 obtain reasonably homogenous pool of MVs having size in the range of 50-150 nm. We
127 optimized the method that allowed us to isolate bacterial MVs without the usage of
128 ultracentrifugation. However, we also isolated the bacterial MVs by using
129 ultracentrifugation method to compare the MVs isolated by chemical vesiculation method.
130 Briefly, bacterial cells were cultured in Luria Bertani (LB) broth by inoculating a single
131 colony of *E. coli* from slant culture. The culture was incubated at 120 rpm at 37°C. Cells
132 were grown until optical density (OD) of culture reached to a value of 1.0 where,
133 considered as the *E. coli* are in mid-exponential phase of growth. Cells were harvested
134 from media by centrifugation at 5000 rpm for 10 minutes at 4°C then supernatant were
135 discarded. The pallet was re-suspended in 50 mL Membrane vesicle (MV) buffer (pH-7.4).
136 Cells were again centrifuged at 5000 rpm for 10 minutes and washed twice in MV buffer
137 to remove remaining media. Pellet of bacterial cells was then resuspended in 30 ml of 3mM
138 of N-ethyl-maleimide (NEM) solution. N-ethyl maleimide (NEM) is well optimized
139 chemical vesiculant for obtaining Giant Plasma Membrane Vesicles (GPMV) from
140 eukaryotic cell membranes. The choice of NEM as a chemical vesiculant is justified by the
141 fact that it is known not to cross-link with proteins and aldehydes or cause coupling of
142 phosphatidylethanolamine to proteins or depalmitoylation. Resuspended cells were
143 incubated in NEM containing MV buffer for 1 hour for vesiculation of bacterial MVs from
144 *E. coli*. Vesiculated bacterial MVs in cells were isolated by high-speed centrifugation at
145 18000g for 2 hours at 4˚C and supernatant containing membrane vesicles (bacterial MVs)

146 was collected. The bacterial MVs in supernatant was concentrated by using a 10 kD cut-
147 off filter through 0.22 µm filter paper for the uniformity in size of bacterial MVs. For
148 conventional method for isolation of MVs by ultracentrifugation method, *E. coli* were
149 grown by inoculating from single colony at 120 rpm up to OD reached ~ 1.0. The cells
150 were pelleted, and supernatant was discarded subsequently, bacterial cell was resuspended
151 in PBS buffer. Again, the cells were centrifuged at 5000 rpm for 10 minutes at 4°C
152 temperature. Supernatant was collected and filtered through 0.22 µM by using vacuum
153 filtration system. Filtered solution contains MVs and were then ultracentrifuge at 100000
154 g for 3 hours at 4˚C. The pellet obtained resuspended in 1 mL of PBS having bacterial
155 MVs. Isotherm analysis for interaction studies of bacterial MVs with cells and reconstituted
156 bio-mimicking model membrane systems. Lipid molecules from bacterial MVs were
157 isolated using the Folch method [11]. 300 µL of freshly prepared MV solution in MV buffer
158 was dried with nitrogen gas stream and kept in vacuum chamber overnight for buffer
159 evaporation. 300 µL chloroform was then added to the dried bacterial MVs and bath
160 sonicated for 30 minutes at constant pulse of 1sec. Post sonication, the solution was
161 transferred to another vial and again dried with nitrogen gas. Chloroform (320 µL) and ice-
162 cold methanol (160 µL) were subsequently added in 2:1 v/v ratio to dried sample and
163 incubated for 20 minutes on ice with occasional vortex mixing followed by addition of 150
164 µL deionized water and kept on ice for additional 10 minutes with occasional agitation.
165 The mixture was then centrifuged at 1500 rpm for 5 minutes for removal of the upper polar
166 phase containing salts and proteins. For additional washing, 2:1 v/v chloroform and ice-
167 cold methanol was again added, and the above process was repeated. After removal of the
168 upper phase, the final lower organic phase containing lipids was dried with nitrogen stream
169 and suspended in 100 µL chloroform. It was kept at -20ºC for future use. Extracted lipid
170 estimation of bacterial MVs is shown in the supporting text [11].

171 **Size Distribution, Detection and Fluorescence Microscopy of MVs**

172 The detection and size of purified bacterial MVs was confirmed by fluorescence
173 microscopy and dynamic light scattering (DLS) experiments. Fluorescence imaging and
174 fluorimetry were done by incorporating a membrane binding dye Nile red to bacterial MVs.
175 In sample preparation for imaging and fluorimetry, 990 µL of bacterial MVs in MV buffer

176 were incubated with 10 µL of Nile red (100 µM) in 100/1 (v/v) ratio of MV/dye for 30
177 minutes. For control sample to perform fluorimetry for Nile red in MV was done by taking
178 10 µL dye in 990 µL of MV buffer. For fluorescence imaging 10 µL of Nile red labelled
179 bacterial MVs were dropped on coverslip to visualize MV under fluorescence microscope
180 (Olympus, IX71) with oil immersed 63x magnification of objective. Fluorescence intensity
181 measurements of bacterial MVs were carried out by checking fluorescence intensity of Nile
182 red incorporated bacterial MVs in MV buffer with respect to control sample i.e., MV buffer
183 with Nile red. Excitation and emission spectra were optimized at 530 nm and 570 nm
184 respectively.

185 For size distribution of bacterial MVs, 1 mL of MV in MV buffer were filled in quartz
186 cuvette and allowed to be equilibrated for 5 minutes. DLS was measured by Zetasizer Nano
187 ZS (Malvern Zetasizer Nano ZS90, Netherland) with 633 nm Laser by electrophoretic
188 mobility of bacterial MVs in solution.

189 **Electron Microscopy of Bacterial MVs**

190 To visualize the morphology of bacterial MVs, we performed transmission electron
191 microscopy (TEM). For TEM analysis of isolated MVs, we fixed the MVs with 1%
192 glutaraldehyde for 2 hours at 4°C. Fixed samples were negatively stained with 2% Uranyl
193 acetate followed by washing twice. The stained MVs kept in vacuum for dehydration of
194 sample and visualized under JEOL F200 equipped with Gatan camera.

195 **Fluorescence Labelling of Bacterial MVs with DiO and Di-8-ANEPPS**

196 Purified bacterial MVs were labelled with a lipophilic dye DiO (3,3'-
197 Dioctadecyloxacarbocyanine Perchlorate) and Di-8-ANEPPS to study affinity/fusion of
198 bacterial MVs with reconstituted membranes. Both dyes mixed to MVs in ratio of 1:100
199 v/v dropwise with constant stirring at 37°C for 30 minutes for incorporation of dye in
200 bacterial MVs. To separate unlabelled dye from labelled bacterial MVs, the mixture was
201 washed PBS buffer four times using 10kD cut-off concentrators (Merck-Millipore) and
202 dialyzed against PBS by changing the buffer twice. Labelled bacterial MVs were kept at
203 4°C and can be stored up to one week for further experiments.

204 **Fusion of Bacterial MVs to Macrophage Cells**

205 To check the fusion of bacterial MVs with macrophages cells, fluorescence intensity was
206 measured. Differentiated macrophages (THP-I) were freshly cultured in RPMI media from
207 the maintained culture. Cells were grown up to 70% of confluence. Cells were washed with
208 2 mL PBS (pH – 7.4). Further, cells were washed with the 2 mL of PBS buffer containing
209 bacterial MVs to monitor binding and fusion of MV in cells and observe the internalization
210 of MVs after 2.5 hours. For sample preparation for fluorimetry to examine fusion of MVs
211 with cells, 100 µL of cell soup was taken, re-suspended in 900 µL of MV buffer and 10 µL
212 of Nile red. For control only 100 µL of MV, 900 µL of MV buffer and 10 µL of Nile red
213 was mixed. Fluorescence intensity was then measured at 530 nm of excitation spectrum
214 and 570 emission spectra in UV-visible spectrophotometer at time t=0. The same samples
215 were scanned for 2.5 hours with 30 minutes of interval for fusion studies.

216 **Reconstitution of Fluorescence Labelled Giant Unilamellar Vesicles (GUVs)**

217 Giant unilamellar vesicles (GUVs) were prepared using polyvinyl alcohol (PVA) gel-
218 assisted method as previously described by Weinberger *et. al.* with slight modifications [12].
219 PVA-coating on the surface of glass slides were used as film for swelling of lipid film for
220 reconstitution of GUVs. To prepare PVA coated slides, PVA was dissolved in deionized
221 water in 5% w/w ratio of PVA/water with constant stirring at 90°C. From this PVA
222 solution, 200-300 µL is evenly spread on the glass slide and dried in oven at 50°C for 30
223 minutes which makes a thin film over the surface of slide. This dried PVA-coated slides
224 then cleaned with UV for 15 minutes to prevent dewetting of PVA coating. Now, 20 µL of
225 Lipid solution in chloroform (1mg/mL) doped with 1 mole % Rhodamine-PE of total lipid
226 mole fraction was smeared on a PVA-coated slide using a Hamilton syringe. Residual
227 chloroform on the PVA-coated slide was Evaporated by keeping the slide in vacuum
228 chamber for 2 to 3 hours. A chamber on the lipid spread PVA-coated slide was made using
229 nitrile ring sealed by using a second coverslip and clips as sealant. This lipid film was then
230 swelled by filling the chamber with 1 mL of 10 mM phosphate buffer saline (PBS) at pH
231 of 7.4 for vesiculation. The buffer used for hydration as well as the buffer with the
232 suspended MVs were adjusted for equi-osmolarity. After 30 minutes the chamber was

233 gently agitated, and the buffer of chamber was collected in microcentrifuge tubes
234 containing GUVs.

235 **Confocal Fluorescence Microscopy**

236 Custom made open chambers were used for incubating the Rhodamine-PE-GUVs and DiO
237 -MVs and NBD-PE-GUVs and Di-8-ANEPPS. The cover slip was rinsed with 70% ethanol
238 and air-dried. 10 µL of the GUVs from the was added to 90 µL of equi-osmolar MV buffer
239 and 1mg/mL bacterial MVs were injected, and samples were incubated for 15-20 mins and
240 allowed to equilibrate and binding of MVs. Imaging was performed using a Leica TCS-
241 SP8 confocal instrument using appropriate lasers for rhodamine-PE (DPSS-561) and DiO
242 (argon-488). An identical laser power and gain settings were used during the course of all
243 the experiments. The image processing was done using ImageJ.

244 **Preparation of Large Unilamellar Vesicles (LUVs)**

245 Each specific type of LUV was prepared with the help of different phospholipids in total
246 number of 120 nmoles by corresponding lipids dissolved in chloroform. The mixture of
247 lipids was doped with 1 mole% of di-8-ANEPPS and for background correction only lipids
248 were mixed free of dye. The prepared mixtures then dried with steady nitrogen gas stream
249 and kept in vacuum for 3 hours for complete evaporation of residual solvent from the lipid
250 mixtures. Thereafter, lipids were re-suspended in 500 µL of MV buffer (pH- 7.4) for
251 hydration of lipids then suspension was heated in water bath for 15 minutes at 45 ºC. After
252 heating, samples were vortexed for 5 minutes and sonicated for 2 minutes at 0.9 sec pulse
253 rate and 100% amplitude to produce LUVs of roughly 500 nm diameter which was
254 confirmed by dynamic light scattering (DLS).

255 **Anisotropy and Dipole Potential Measurement of Reconstituted Membranes**

256 Anisotropy and dipole potential measurements of specific lipid membranes were done by
257 fluorescence spectroscopy. For these studied, reconstituted LUVs with specific
258 composition of phospholipids were used and incubated with bacterial MVs. For each
259 sample preparation, 200 µM of LUVs without bacterial MVs was taken as control whereas
260 the same sample treated with 0.2 mg/mL and 0.6 mg/mL of bacterial MVs were the test

261 samples. Now, these samples were incubated for 1 hour at 25°C in dark before fluorometric
262 quantification i.e., anisotropy and dipole potential measurements. All measurements were
263 done in 500 µL of quartz cuvette by using LS55 PerkinElmer spectrophotometer. For
264 dipole potential study, excitation spectra were obtained by scanning the sample with 5 nm
265 slit bandpass at 240 nm/s scan speed and the emission wavelength was fixed at 670 nm to
266 avoid membrane fluidity effects. Background was corrected by subtracting the intensities
267 of test samples containing di-8-ANEPPS with sample without the dye. Dipole potential
268 was calculated by taking ratio (R), of emission intensities at 670 nm excited at 420 nm and
269 520 nm respectively for each sample. All values of anisotropy were calculated
270 automatically by the instrument by using the following equation (1)[13]:

271 $$r = \frac{I_{VV} - GI_{VH}}{I_{VV} + 2GI_{VH}} \quad (1)$$

272

273 Where, I_{VH} and I_{VV} are the measured fluorescence intensities with excitation polarizer
274 oriented vertically and emission polarizer oriented horizontally and vertically, respectively.
275 G (= I_{HV}/I_{HH}) is the grating correction factor and is the ratio of the efficiencies of the
276 detection system for vertically and horizontally polarized light. All experiments were
277 conducted with multiple independent sets for each lipid.

278 **Lipid Mixing Experiment performed with labeled liposomes**

279 Fusion between LUVs of outer leaflet model membrane (OLMM-RhodPE) composed of
280 (DOPC 35.7 mole%, DOPE 5.5 mole %, SM 19.2 mole%, and Cholesterol 31.3 mole%)
281 labeled with NBD-PE/Rh-PE (0.8 mol% each) and unlabeled bacterial MVs were
282 monitored by the NBD fluorescence. The kinetics of lipid transfer from LUVs to MVs
283 through FRET dilution was measured as a function of time. The lipid transfer during vesicle
284 fusion was monitored using the change in FRET efficiency between NBD-PE (donor) and
285 Rh-PE (acceptor). The emission intensities of the donor were monitored in 96 well
286 Clariostar micro plate reader with excitation and the emission wavelength monochromator
287 set to 465 nm and 530 nm, respectively. Each experiment was repeated at least three times.
288 The extent of lipid mixing was calculated using following equation (2):

289

290 $$\%LipidMixing = \left(\frac{F_t - F_0}{F_\infty - F_0}\right) * 100 \quad (2)$$

291 where 'F_0' is the initial fluorescence, 'F_t' is the fluorescence after t minutes of incubation,
292 and F_∞ is the value of fluorescence after addition of TX-100 (1%) to dissolve the liposome,
293 which is considered as the maximum disperse of the probe [14].

294 **Langmuir Blodgett Monolayer Preparation and Isotherm Analysis**

295 Langmuir monolayer films were prepared using a microprocessor-controlled Teflon
296 molded LB trough (Apex Instruments, India) having inner working dimension of 305 mm
297 X 105 mm. The rectangular trough was equipped with two movable Teflon bars which
298 provided symmetrical compression speed and the surface pressure being measured with an
299 accuracy of ±0.05 mN/m by a Wilhelmy plate (filter paper of dimensions 10 x 25 mm^2)
300 connected to a highly sensitive electronic balance system. The entire system was set inside
301 a transparent glove box. The trough was cleaned subsequently with methanol, ethanol and
302 ultrapure water to make it dust free and utmost care was taken to avoid internal and external
303 vibration during the experiments. MV buffer was used as the subphase whose temperature
304 was maintained at 25 ºC. Prior to each isotherm run, the interface cleaning operation was
305 performed by compressing the two bars to a maximum and checking the surface pressure.
306 Lipid solution at 1 mg/ml concentration was spread drop by drop on the air/ buffer interface
307 until a surface pressure of 2-3 mN/m was reached and waited for 15-20 minutes for the
308 chloroform to evaporate off and π to come down to 0 mN/m. 10 µL MV solution (2 µM)
309 was injected into the subphase prior to monolayer compression. The subphase was
310 constantly agitated using a magnetic bead stirrer at the bottom of the trough for uniform
311 distribution of bacterial MVs. π-A Isotherm run was started by compressing the monolayer
312 at a constant speed of 8 mm/min. Isotherms were recorded until collapse pressure π_c was
313 reached. Thorough cleaning of the trough was followed each run. Each isotherm was
314 repeated independently to ensure consistency. Isotherm data were used to calculate
315 compressibility modulus (C_s^{-1}), excess Gibb's free energy of mixing (DG_{Excess}) and bending
316 force (ΔF_b).

317

318

319 ## Statistical Analysis

320 Data were analyzed by one-way analysis of variance (ANOVA) using Origin 8.5 software.
321 *p-values* < 0.5 were considered were considered statistically significant. All values were
322 reported as mean ± SE from appropriate sample size and three independent experiments as
323 indicated and where (***) depicts p<0.001, (**) p<0.01 and (*) p<0.05.

324 ## Results

325 ### Bacterial membrane vesicle (MV) fusion increases the fluidity and dipole potential of
326 host lipid membrane

327 Bacterial membrane vesicles have been reported to enter host cells via multiple routes such
328 as endocytosis, micropinocytosis and fusion in different cell types [15]. Here, we sought to
329 elucidate the lipid specificity and modulation of host membrane properties by bacterial MV
330 interaction which remains central to all routes of entry yet remains unexplored. We used
331 *E. coli* as a model Gram negative bacterium for the isolation of bacterial MVs and set out
332 to systematically investigate the interaction of bacterial MVs with host membranes (***Fig.***
333 ***1A***). Bacterial MVs were isolated by means of chemically induced vesiculation, which in
334 comparison to the usual ultracentrifugation-based isolation, yield a relatively homogenous
335 size of MVs. The characterization of the size heterogeneity of bacterial MVs was carried
336 out by electron microscopy, fluorescence-based pixel size estimate and dynamic light
337 scattering. Electron microscopy of MVs (***Fig. 1B, Fig S1A-S1D***) showed that MVs isolated
338 by ultracentrifugation-based method had a broad size range of ~ 50-200 nm (***Fig. 1C***),
339 unlike, chemically induced vesiculation method that yield MVs with diameter of ~ 50-60
340 nm (***Fig. 1C, Fig S1***). The same was found to be ~ 150 nm by dynamic light scattering
341 (***Fig. 1D, Fig S1E***). Further, we labelled bacterial MVs with fluorescent lipophilic dyes -
342 such as 3,3′-dioctadecyloxacarbocyanine perchlorate (DiO) (***Fig. 1E***), Nile red and Di-8-
343 ANEPPS to monitor binding and visualization of MV fusion by confocal microscopy as
344 they are known to fluoresces only under lipid-rich environment [16].

345

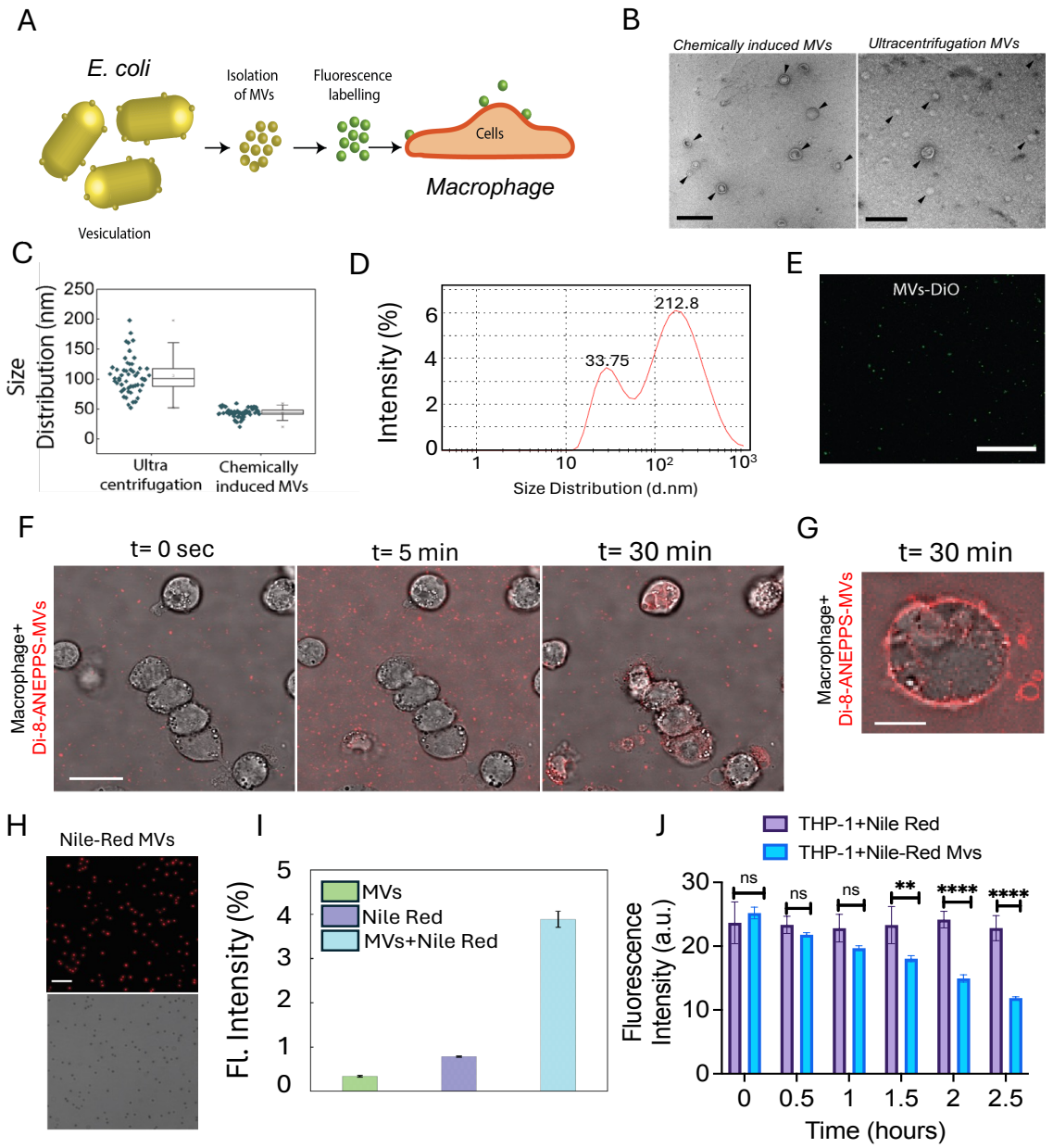

346

347 ***Figure 1.*** **Characterization of bacterial Membrane Vesicles (MVs) isolated from**
348 ***Escherichia coli*** **and internalization of bacterial MVs in macrophages. A)** Schematic
349 summarizing the methodology used to isolate, fluorescently label and study the MV-host
350 membrane interaction. **B)** TEM micrograph of MVs isolated through chemical vesiculating
351 and ultracentrifugation method (scale bar – 500 nm). **C)** Box plot for size distribution of
352 MVs obtained through TEM micrographs. **D)** Plot showing size distribution of MVs by
353 DLS method. **E)** Confocal image of DiO labelled MV suspension (Scale bar - 10 µm). **F)**

354 Time-course confocal sections showing fusion and internalization of Di-8-ANEPPS
355 labelled MVs (red fluorescence) in differentiated macrophages- THP-I cells. Scale bar is
356 25 µm. **G)** Image from a different plane of THP-I cells with Di-8-ANEPPS after 30 minutes
357 of incubation. Scale bar is 20 µm. ~10-12 cells were visualized under the microscope. **H)**
358 Fluorescence image of MVs labelled with Nile red dye (scale bar is 10 µm). **I)** Bar plot
359 depicting fluorescence intensity of MVs (without Nile Red), Nile red only, and MVs
360 labelled with Nile Red. **J)** Histogram showing fluorescent intensity measurements of Nile
361 red incubated with macrophages and Nile Red-MVs incubated to differentiated
362 macrophages with increasing at different time-points to confirm fusion of MVs to host cell.
363 Values are mean intensity ± S.E. Significance was determined by one-way ANOVA with
364 indicating significant difference; ns= non-significant, **p < 0.01, ***p <0.001, ****p
365 <0.0001.

366 We then confirmed the interaction of bacterial MVs by human macrophages using
367 differentiated THP-1 cells wherein significant internalization of the Di-8-ANEPPS labelled
368 MV can be seen inside the macrophage after 30 minutes of incubation (***Fig. 1F-1G***) [9, 17].
369 Additionally, the labelled bacterial MVs (devoid of any free unbound dye) were incubated
370 with the THP-1 cells in cell media for a period of about 2.5 hours at 37˚C to monitor the
371 changes in the bacterial MV fluorescence arising in the cell media. Measurement of
372 fluorescence intensity of a fixed volume of isolated cell media every 30th minute revealed
373 a gradual yet linear decrease in the fluorescence arising from the residual labelled MV (***Fig.***
374 ***1I***). This methodology also provides an indirect measure of the kinetics of the bacterial
375 MV fusion with the macrophage cells. Fluorescence bleaching can be ruled out as no
376 significant change in fluorescence of the cell media containing MV was observed in the
377 absence of macrophage cells (***Fig. 1J***).

378 Previous investigations have reported that Bacterial MVs not only associate with the host
379 cell surfaces but also incorporate with different phospholipid liposomes in vitro[9].
380 Irrespective of the kind of bacterial MV, the interaction of the bacterial MVs takes place
381 with the outer leaflet of the host lipid membrane. To this end, we reconstituted giant
382 unilamellar vesicles (GUVs) comprising the predominant lipids of the outer leaflet of a
383 eukaryotic cells (i.e., DOPC 35.7 mole%, DOPE 5.5 mole %, SM 19.2 mole%, and

384 Cholesterol 31.3 mole%), in order to mimic the outer leaflet model membrane (OLMM)
385 of host cell membrane[18].

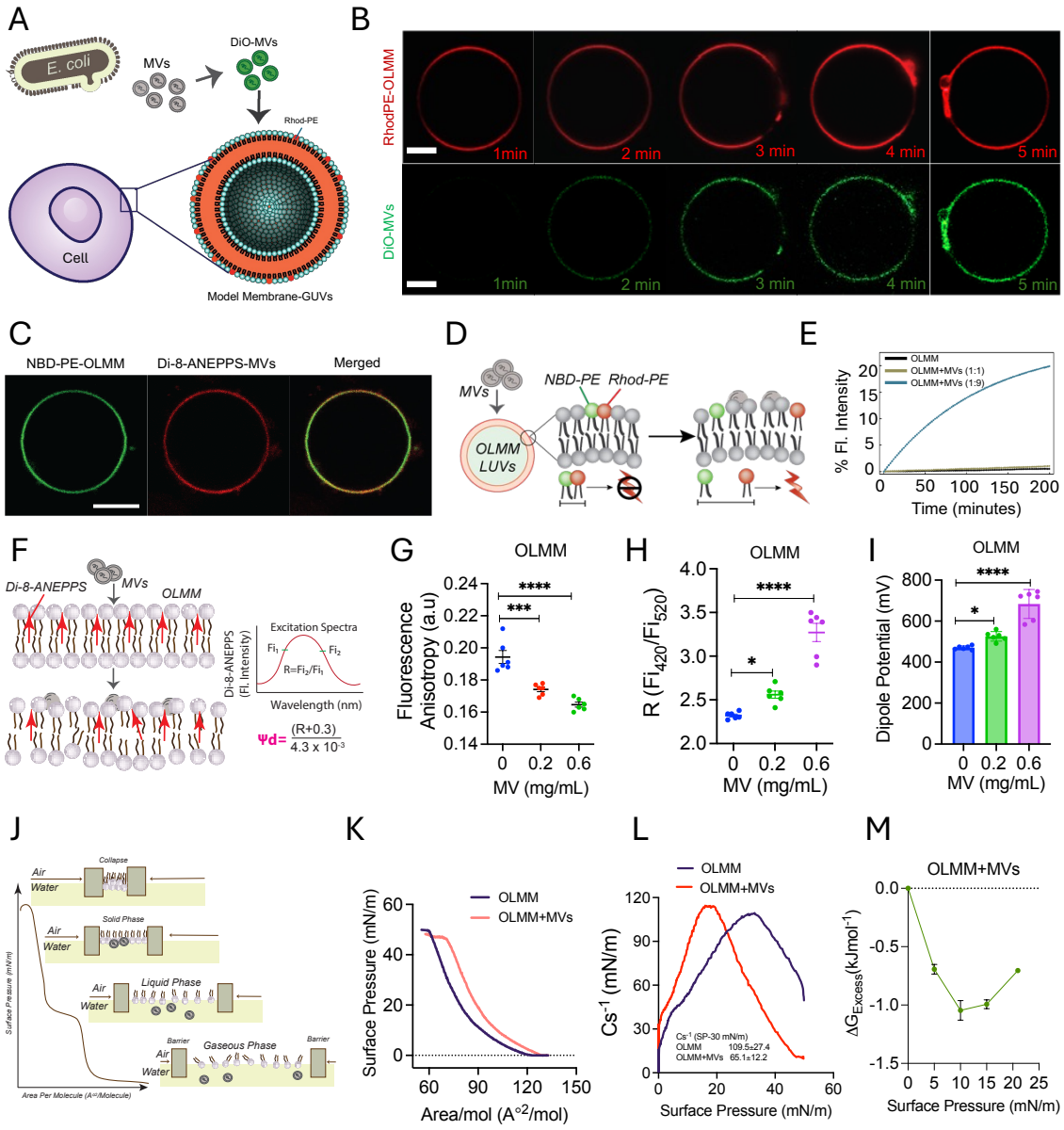

386

387 ***Figure 2.*** **Bacterial membrane vesicles (MVs) binds to host model membrane and**
388 **alters biophysical parameters of host lipid membrane. A)** Model depicting the approach
389 to study binding of fluorescently labelled-MVs with host lipid model membrane (Giant
390 Unilamelar Vesicles). **B)** Confocal images of reconstituted GUVs of outer leaflet model
391 membrane (OLMM-RhodPE) composed of (DOPC 35.7 mole%, DOPE 5.5 mole %, SM
392 19.2 mole%, and Cholesterol 31.3 mole%) doped with 1 % Rhodamine PE (*red channel*)

393 mimicking outer leaflet of eukaryotic cell membrane. Bacterial MVs labelled with DiO
394 binding to the GUVs (green channel) distributed homogeneously over the equatorial plane
395 of GUVs along with merged image of both red and green channels showing a co-
396 localization. **C)** Confocal sections showing the distribution of Di-8-ANEPPS-MVs (red
397 fluorescence over the host lipid membrane NBD-PE-OLMM (green fluorescence). .
398 Fluorescence imaging was done thrice independently and at least 30-35 GUVs were
399 observed under microscope (scale bar - 10µm). **D)** Illustration is showing experimental
400 design of FRET assay for MVs-OLMM mixing. LUVs (outer leaflet) doped with
401 quenching dye pair- NBD-PE and Rhodamine-PE and incuabted with MVs and fusion of
402 MVs would increase Intermolecular distance of both dye and fluorescence intensity will
403 increase. **E)** Lipid mixing kinetics of labeled LUVs with bacterial MVs at 37 ºC. An
404 increase in NBD fluorescence implies fusion between LUVs and MVs as compared to
405 control. All measurements were carried out in PBS buffer, pH 7.4. The values represent
406 means of at least three independent experiments performed in triplicate ± S.E. **F)** Schematic
407 diagram depicting intercalating of charge-shift probe Di-8-ANEPPS to the cell membrane
408 and excitation spectra showing changes in the orientation of the probe in the membrane
409 bilayer. **G) and H)** Fluorescence intensity ratio at 420/520 nm of wavelength and dipole
410 potential of the outer leaflet model membrane incubated with increasing concentration of
411 Bacterial MVs, increased at high concentration of Bacterial MVs. **I)** Fluorescence
412 anisotropy of OLMM decreases with increasing concentration of bacterial MVs correlating
413 with the increased fluidity of host model membrane. **J)** Model showing Langmuir-Blodgett
414 set up for lipid monolayer formation and phases of monolayer with compression. MVs
415 injected in water subphase to observe effect on OLMM. **K)** Surface Pressure (π) - Mean
416 molecular area (A) isotherm of OLMM monolayer (black curve) and OLMM incubated
417 with bacterial MVs (red curve) showing right shift. All isotherms were compressed with
418 constant speed of 8 mm/minute at 25 °C temperature. **L)** Compressibility modulus (C_s^{-1})
419 with respect to surface pressure of OLMM monolayer (black curve) and OLMM with MV
420 (red curve) showing decreased C_s^{-1} on the air-water interface. **M)** Excess Gibb's free energy
421 of mixing between OLMM and bacterial MVs shows an ideal mixing and decrease with
422 increasing surface pressure calculated from Langmuir isotherms. All fluorescence
423 spectroscopic data are shown as mean ± S.E. from three independent experiments.

424 Significant variations were compared through one-sided ANOVA of OLMM treated with
425 0.2 mg/mL and 0.6 mg/mL of Bacterial MVs with respect to control, where, (***) depicts
426 $p<0.001$(**) $p<0.01$ and (*) $p<0.05$, data point with 'ns' mark are not significant. All
427 representative isotherms are the mean of independently performed experiments. For
428 isotherms and compressibility modulus curves the estimated standard error for data points
429 of surface pressure (π) with respect to area per molecule (A) was approximately ±0.05
430 mN/m.
431 To corroborate the MVs binding to OLMM, we labeled GUVs with Rhodamine-PE
432 (emission wavelength, 576 nm) and bacterial MVs with DiO (emission wavelength, 501
433 nm). The binding of DiO labelled bacterial MVs was observed with the outer leaflet model
434 membranes (OLMM) (***Fig. 2B***). To rule out the passive membrane incorporation
435 equilibrium of DiO, we labelled the large unilamellar vesicle of DOPC with DiO as a
436 control and incubated with outer leaflet model membrane (OLMM).

437 No binding or fusion of DiO-DOPC to host model membrane was observed as monitored
438 by confocal microscopy (***Fig. S2***). On the contrary, we investigated the MVs binding by
439 labelling the MVs with membrane incorporating dye – Di-8-ANEPPS and GUV comprised
440 of the outer leaflet lipids of the host membrane by NBD-PE. To rule out bleed-through due
441 to wide spectra of Di-8-ANEPPS, we limit the emission bandwidth of Di-8-ANEPPS to
442 10% of NBD-PE excitation, which would minimize the spectral overlap of both dyes (***Fig***
443 ***S8***). The homogenous distribution of MVs over the equatorial plain of the of NBD-PE-
444 OLMM GUV suggests significant interaction of MVs with host lipid membrane (***Fig. 2C***).
445 Furthermore, The binding of bacterial MVs to the host membrane mimic comprising outer
446 leaflet lipids as well as THP1 cells appeared to take place within 30 minutes as reported
447 earlier in different cell lines [19].

448 The fusion of bacterial MVs with membranes was further established using the
449 Fluorescence resonance energy transfer (FRET) between labeled LUVs and bacterial MVs.
450 We used the fluorescent FRET pair NBD-PE and Rh-PE, where enhancement in donor
451 (NBD-PE) fluorescence intensity shows lipid mixing taking place between the two vesicles
452 indicating fusion (***Fig 2D***). To examine the fusion event, we have taken two different ratios
453 of probed LUVs (i.e., containing the FRET pair) with MVs to monitor the maximum fusion

454 at 37ºC and at neutral pH 7.4. Fusion between probed LUVs and unprobed LUVs was
455 monitored as a control which showed no significant change in donor fluorescence even
456 after incubation for 3-4 hours. The probed to unprobed (LUV:MV, 1:1) membrane system
457 showed only ~1% maximum lipid mixing. A ratio of 1:9 has previously been reported and
458 widely used for such membrane fusion assays[20] and upon taking probed LUV and unprobed
459 MVs in 1:9 ratio, a lipid mixing of ~20% was observed as shown in ***Fig. 2E***. The time
460 course of lipid mixing is much significant when MV concentration is higher, which
461 indicates probed vesicles get fused with bacterial MVs. This is expected as the probability
462 of interaction of MVs with the host membrane would increase with the number of MVs
463 secreted and the amount available in the vicinity of the host membrane for random collision
464 and interaction

465 We next sought to investigate whether the interaction of the bacterial MVs with the host
466 membrane results in changes in the fluidity and dipole potential (Ψ_d) of the host membrane
467 (***Fig. 2F***). The changes in membrane fluidity were quantified by reconstituting a
468 potentiometric styryl membrane probe di-8-ANEPPS (Pyridinium, 4-[2-[6-(dioctylamino)-
469 2-naphthalenyl]ethenyl]-1-(3-sulfopropyl)), with membrane vesicles, whose fluorescence
470 anisotropy (a measure of rotational relaxation time) responds to the changes in the
471 dynamics of the membrane environment (***Fig. 2F***). The fluorescence anisotropy of the host
472 outer leaflet model membrane was found to decrease by ~ 9 % upon MV interaction
473 suggesting increased fluidization of the host membrane (***Fig. 2G***). Likewise, the probe di-
474 8-ANEPPS, is known to undergo shift in the fluorescence excitation spectrum in linear
475 response to dipole potential changes in the lipid environment, which in turn, is dependent
476 on the electric field in the membrane environment [13, 21, 22]. The dipole potential of the host
477 outer leaflet model membrane was found to increase by ~ 67 % suggesting strong local
478 remodeling upon the interaction of MV (***Fig. 2H-2I***). The dipole potential originates from
479 the non-random arrangement of molecular dipoles (i.e., water, carbonyl-groups and lipid
480 head-groups) at the membrane interface [22]. Further, the surface zeta potential of the
481 bacterial MVs was found to be ~ - 9 mV and that of the outer leaflet model membrane lipid
482 components was also found to be negative, however, of higher magnitude (- 20mV to -

483 25mV) as compared to bacterial MVs (Table S1).

484 **Bacterial MV fusion increases the Compressibility and facilitates bending of host**
485 **model membrane**

486 After establishing the internalization of MVs in cells as well as binding and fusion with
487 host model membranes, estimating the accompanied changes in the fluidity and dipole
488 potential of the host membranes, we further sought to quantify the changes in the
489 Compressibility of the host membrane. Langmuir monolayer surface area-pressure
490 isotherms are a powerful means that enable quantification of the thermodynamic aspects
491 of the MV interaction with the host model membranes and the associated changes in
492 physicochemical properties of the host membranes[23]. We first investigated the surface
493 pressure-area (π-A) isotherms (***Fig. 2J***) for the outer leaflet model membrane (OLMM).
494 OLMM being a complex multi-component lipid mixture only showed liquid-expanded (L_e)
495 and -condensed (L_c) behaviour, without any significantly evident 2D phase transition (***Fig.***
496 ***2K***). Marked increase in the area per molecule with increasing surface pressure was
497 observed, in the presence of MV in the sub-phase suggesting significant interaction and
498 fusion between the monolayer membrane and bacterial MVs (***Fig. 2K***). To further
499 corroborate our conclusions, the changes in the host model membrane surface
500 compressional modulus, C_s^{-1} (i.e., reciprocal of surface compressibility or Compressibility,
501 C_s), were extracted using the slopes obtained from (π-A) isotherms. Compressibility
502 modulus, C_s^{-1}, is related to the change in surface pressure and area per molecule, as defined
503 in equation (3) -

504 $$C_s^{-1} = -A\frac{d\pi}{dA} \quad (3)$$

505

506 and is known to be very sensitive to subtle changes in lipid structure during lateral
507 interaction and thus, provides molecular insights into lateral packing Compressibility of
508 the host membrane [24]. Upon the fusion of bacterial MVs, the monolayer compressibility
509 modulus was found to have decreased by ~ 44 mN/m (***Fig. 2L***), particularly nearing a
510 surface pressure of ~30 mN/m which has been established to possess identical chemical
511 potential and molecular area to that of bilayers in equilibrium [25]. Further, the excess Gibbs

512 free energy of mixing of bacterial MVs with OLMM was calculated at certain surface
513 pressures by integrating the excess area over surface pressure, and denoted by the equation
514 (4) [26] -

515 $$\Delta G_{Excess} = \int_0^{\pi} [A_{12} - (X_1 A_1 + X_2 A_2)] d\pi \quad (4)$$

516 where, A_{12} is the mean molecular area occupied by the mixed monolayer in the presence
517 of MV, A_1 and A_2 are the mean molecular areas occupied by monolayer and bacterial MVs
518 respectively, and X_1 and X_2 are the molar fractions of the monolayer component and
519 bacterial MVs respectively. ΔG_{Excess} showed a decreasing trend with increasing surface
520 pressure suggesting the mixing of MV with monolayer lipids to be more favourable till a
521 surface pressure at 10 mN/m whereas slight increase was observed at 15 mN/m and
522 20mN/m (***Fig. 2M***), as the maximum crowding of bacterial MVs approached as reflected
523 in the (***Fig. S4***). The difference of the collapse pressures (π_c) of monolayer membranes in
524 the presence and absence of MV depicts the change in lateral bending force (ΔF_b) acting
525 on the monolayer during the fusion which was calculated using the equation (5):

526 $$\Delta F_b = MM.MV\pi_c - MM\pi_c \quad (5)$$

527 where, $MM.MV\pi_c$ is the collapse pressure of model membrane with bacterial MVs in
528 subphase and $MM\pi_c$ being without bacterial MVs. Negative values of (ΔF_b) suggest
529 bending of monolayer [27]. The (ΔF_b) was found to be ~ -1.75 mN/m suggesting the
530 feasibility of bending upon fusion of bacterial MVs (***Table S2***). In addition, we also
531 examined the π-*A* isotherms of the MV components (i.e., lipopolysaccharides,
532 phospholipids devoid of any proteins) extracted from bacterial MVs (see methods for
533 biphasic solvent extraction for lipids from MVs). A clear gaseous phase was observed in
534 the beginning followed by L_e phase and a short L_c phase just before the collapse at around
535 21mN/m (***Fig. S3A***). The compressibility modulus showed a sharp rise till a surface
536 pressure of 2-3mN/m from which it became constant at a value of 16mN/m. Both lower
537 collapse pressure and constant compressibility modulus suggest a significantly rigid
538 behaviour resisting compression (***Fig. S3B***).

539

540 **Role of host membrane lipid head group in bacterial MV interaction**

541 We next questioned if there is any lipid specific preferential interaction of the OMV with
542 the host cell membrane outer leaflet that majorly contributes towards interaction/fusion of
543 MVs. To probe this, we reconstituted liposomes composed of the major phospholipids
544 present in the outer leaflet of the host cell membrane i.e., DOPC, DOPG, PI and BSM. We
545 analyzed the binding and colocalization of MVs with lipid membranes i.e. DOPC, DOPG
546 and PI, to visualize lipid-MVs interaction (***Fig. 3A***). Significant binding of MVs to all the
547 above lipid membranes was observed as evident from the homogenous DiO signal (green)
548 arising from the equatorial plane of giant unilamellar vesicels (GUVs) colocalizing with
549 Rhodamine PE signal (red) (***Fig. 3A***). After confirming the interaction of MVs with
550 DOPC, DOPG and PI lipids, we further quantified the modulation of dipole potential and
551 fluidity changes in these lipid membranes. We then investigated the role of lipid head group
552 on the MV induced dipole potential changes in the host membrane. We observed that
553 membranes composed of DOPC (***Fig. 3B-3C***), DOPG (***Fig. 3D-3E)*** and PI (***Fig. 3F-3G)***
554 undergo significant changes in their dipole potential (i.e., 21 %, 15 % and 9 % respectively)
555 (***Fig. 3B-3G***) and membrane composed of BSM did not undergo any significant change in
556 the measured dipole potential (***Fig S4B***). On the contrary, we found that DOPC, DOPG,
557 BSM and PI membranes, all undergo significant changes in the membrane fluidity upon
558 the interaction of MVs. Interestingly, the fluorescence anisotropy of the dye was found to
559 decrease in case of DOPC, DOPG and Liver PI by ~ 66 %, 45 % and 45 % respectively,
560 suggesting enhanced fluidization (***Fig 3H-3J***). On the contrary, the membrane composed
561 of BSM showed an increase in the fluorescence anisotropy of the dye by 7 %, suggesting
562 the membrane becoming more rigid (***Fig. S4A***). We then sought to investigate the
563 modulation of membrane elasticity upon MV fusion and mixing with regard to various lipid
564 head-groups. We observed, MV addition caused decrease in area per molecule in case of
565 DOPC (***Fig. 3K***), whereas only slight change in PI (***Fig. 3M***), which remained almost
566 constant with increasing pressure. Coexistence of Lc+Le phase seemed to be very mild in
567 DOPC curve with no clear occurrence in the other two lipids. On the contrary, an increase
568 in the molecular area of DOPG in the presence of MV was observed as evident in the rise

569 in surface pressure (***Fig 3L***).

570

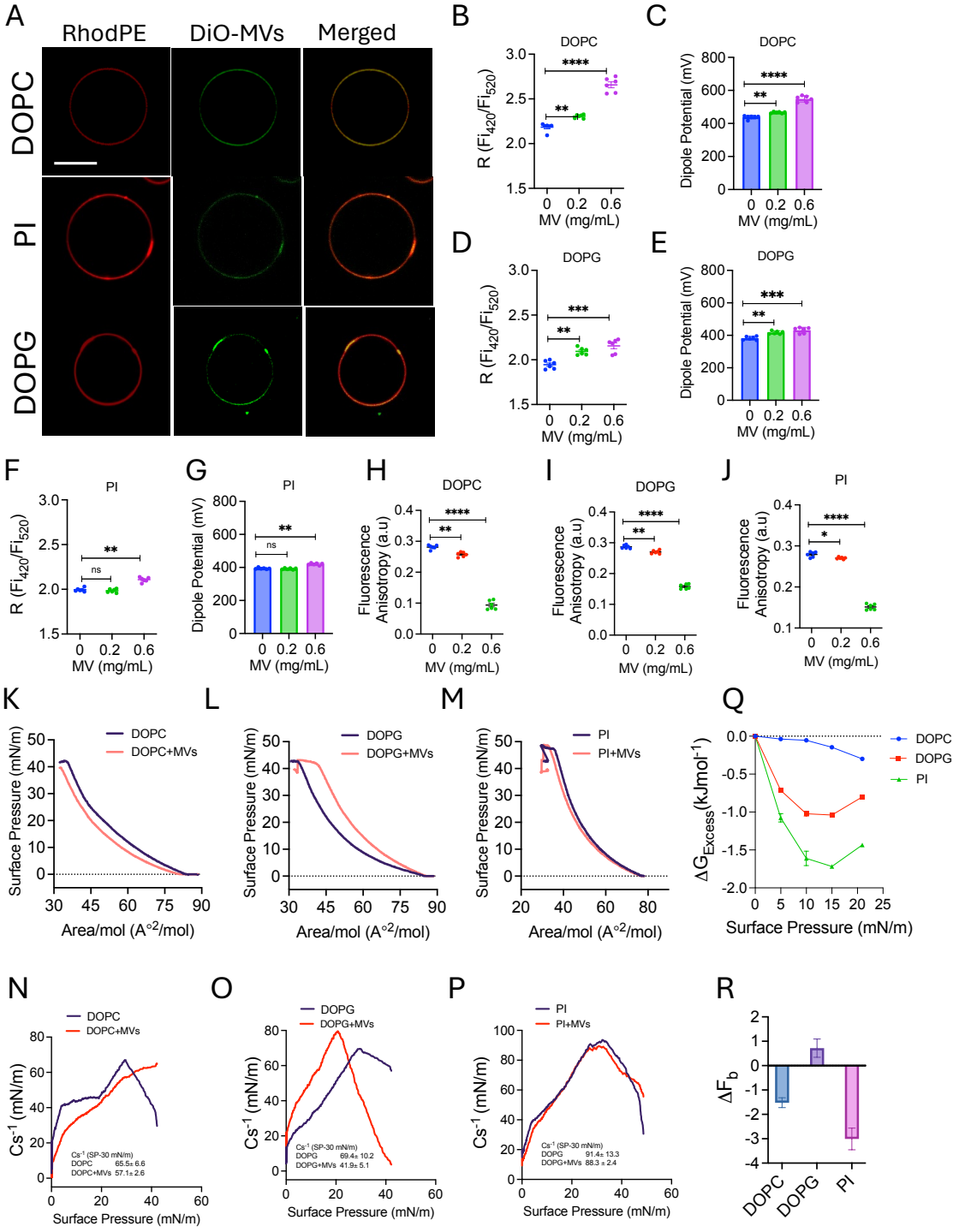

571

572 ***Figure 3.*** **Monitoring the lipid specificity of host membrane for bacterial MVs**
573 **interaction using confocal and the fluorometry of the potentiometric dye, Di-8-**

574 **ANEPPS. A)** Confocal image of DOPC, PI and DOPG doped with 1% Rhodamine PE (*red*
575 *fluorescence)* mixed with bacterial MVs labelled with DiO (*green fluorescence)* to
576 visualize the interaction of bacterial MVs with lipid membrane. A green fluorescence
577 signal on the equatorial plane of membrane suggests the interaction of bacterial MVs with
578 these phospholipids. Fluorescence ratio 420/520 nm and dipole potential (MV) for **B and**
579 **C)** DOPC, **D and E)** DOPG and **F and G)** PI membranes at 0.2 mg/mL and 0.6 mg/mL
580 concentration of bacterial MVs with respect to control model membranes. Membrane
581 anisotropy of **H)** DOPC, **I)** DOPG and **J)** PI with increasing concentration of bacterial MVs
582 i.e., 0 mg/mL, 0.2 mg/mL and 0.6 mg/mL. Measurements for calculation of dipole potential
583 were done at measured intensity at excitation wavelength set at 420 nm and 520 nm
584 respectively. All fluorescence spectroscopic data are shown as mean ± S.E. from three
585 independent experiments. Surface Pressure (π)-mean molecular area (A) isotherms of – **K)**
586 DOPC, **L)** DOPG and **M)** PI monolayers in presence of MVs. Changes in comp ressibility
587 modulus of **N)** DOPC, **O)** DOPG and **P)** PI membrane derived from isotherm of respective
588 model membrane-MVs interactions. **Q)** Variation of excess Gibb's free energy of mixing
589 of bacterial MVs with single monolayers (DOPC, DOPG and PI) as a function of increasing
590 surface pressures 0 mN/m, 5 mN/m, 10 mN/m, 15 mN/m and 20 mN/m. **Q)** Bending force
591 (ΔF_b) histogram of DOPC, DOPG and PI, monolayers at the interface in presence of
592 bacterial MVs. All isotherms were recorded with constant barrier compression speed of 8
593 mm/min at 25°C. All representative isotherms are the mean of independently performed
594 experiments conducted thrice. For isotherms and compressibility modulus curves the
595 estimated standard error for data points of surface pressure (π) with respect to area per
596 molecule (A) was approximately ±0.05 mN/m.
597 A reduction of 1.52 mN/m and 3.01 mN/m in the collapse pressure of DOPC and PI
598 membrane was observed, though DOPG membrane showed a little rise of 0.72 mN/m (***Fig***
599 ***3K-3L***). The negative values of the change in bending force (ΔF_b) suggest bending of
600 monolayer [27] by the interacting MV as observed in case of both DOPC and PI lipid
601 membranes (***Fig. 3R***).
602
603 Further, OMV interaction/fusion induced a reduction in monolayer compressibility
604 modulus (C_s^{-1}) by around ~ 8 mN/m, ~ 28 mN/m and ~ 2 mN/m, in DOPC, DOPG and PI

605 lipid membranes, respectively. (***Fig. 3N-3P***). The reduction in C_s^{-1} in the presence of MV
606 suggests a rise in the membrane monolayer compressibility. We next wanted to see if the
607 mixing of MV with each lipid monolayer is thermodynamically favourable or not. A
608 decreasing negative value trend in ΔG_{Excess} was observed (***Fig. 3Q***) with respect to
609 increasing surface pressure till 15 mN/m in DOPC and PI and 10 mN/m in DOPG after
610 which the curve rose. Upon the mixing of MV, DOPG membrane monolayer showed the
611 lowest free energy change of ~ -1.05 kJ/mol and highest being ~ -1.7 kJ/mol for PI
612 indicating more favourable mixing with PI monolayer.
613

614 **Role of lipid acyl chain in OMV mediated modulation of membrane fluidity, dipole**
615 **potential and elasticity**

616 The lipid acyl chain length is known to determine the membrane bilayer thickness as well
617 as contributes to the degree of fluidity of the membranes [28]. Therefore, we then sought to
618 investigate the role of lipid acyl chain (i.e., C12, C14, C16, C18) of host membrane in the
619 MV mediated changes in the overall host membrane fluidity and dipole potential. The
620 overall fluorescence anisotropy of the dye was found to decrease by ~ 30 % in DPPC
621 suggesting increased fluidization (***Fig. 4C***), and increase by ~ 28 %, ~ 43 % and ~ 27 % in
622 DLPC, DMPC and DSPC respectively, suggesting decrease in fluidity (***Fig. 4A, 4B and***
623 ***4D***). The contrasting observation is noteworthy, as it suggests, that MV interaction seems
624 to enhance the fluidity of a relatively less fluid membrane (such as DPPC, C16) and
625 decrease the fluidity of relatively more fluid membranes (such as C12,14). The observed
626 fluctuations in the fluorescence anisotropy with increasing concentrations of the MV, could
627 hint at a dynamic interaction during the crowding/interaction of the MV. Further, the
628 dipole potential was found to increase in all cases (DMPC, DPPC and DSPC) (***Fig. 4E and***
629 ***4I, 4G and 4K, 4H and 4L***) but decrease in DLPC membranes upon MV interaction (***Fig.***
630 ***4F and 4J***). On the contrary, MV interaction with DLPC membranes resulted in less
631 significant change in the dipole potential. In case of DMPC (***Fig. 4F and 4J***) and DSPC
632 (***Fig. 4H and 4L***), the dipole potential was found to increase by ~ 30% and ~ 15%
633 respectively, at highest concentration of MVs as compared to control which confirms
634 interaction of bacterial MVs with DMPC and DSPC membrane. Likewise, DPPC
635 membrane shows significant increase in dipole potential upon interaction (***Fig. 4G and***

4K).

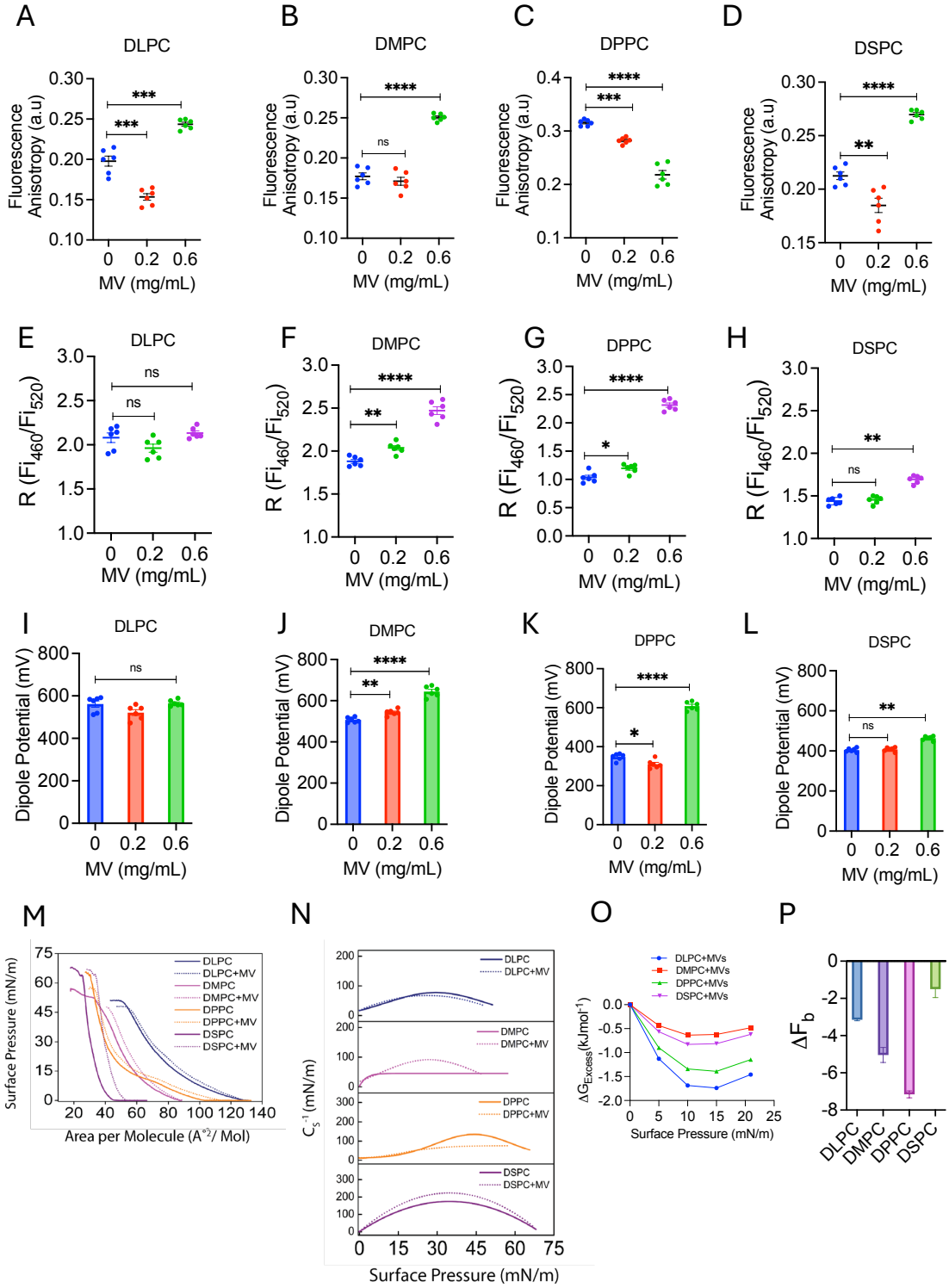
A
DLPC
Fluorescence Anisotropy (a.u)
MV (mg/mL)
B
DMPC
C
DPPC
D
DSPC
E
R (Fi460/Fi520)
F
G
H
I
Dipole Potential (mV)
J
K
L
M
Surface Pressure (mN/m)
Area per Molecule (A*2/ Mol)
DLPC
DLPC+MV
DMPC
DMPC+MV
DPPC
DPPC+MV
DSPC
DSPC+MV
N
Cs-1 (mN/m)
Surface Pressure (mN/m)
O
DLPC+MVs
DMPC+MVs
DPPC+MVs
DSPC+MVs
ΔGExcess(kJmol-1)
Surface Pressure (mN/m)
P
ΔFb
DLPC
DMPC
DPPC
DSPC

639 ***Figure 4.*** **Variation in biophysical properties of phospholipid membranes with**
640 **increasing bilayer thickness as a function of acyl chain length, treated with MVs.**
641 Fluorescence anisotropy of individual lipid model membranes **A)** DLPC, **B)** DMPC, **C)**
642 DPPC, and **D)** DSPC incubated with increasing concentration of MVs. Changes in
643 fluorescence ratio and dipole potential of **E and F)** DLPC, **G and H)** DMPC, **I and J)**
644 DPPC, and **K and L)** DSPC membrane with respect to increasing concentrations of MVs
645 i.e., 0 mg/mL, 0.2 mg/mL and 0.6 mg/mL. All fluorescence spectroscopic data are shown
646 as mean ± S.E. from three independent experiments. Significant variations were compared
647 through one-sided ANOVA of membrane condition treated with MVs with respect to
648 control (only lipid membrane without MVs), where (***) depicts $p<0.001$, (**) $p<0.01$ and
649 (*) $p<0.05$, data point with no asterisk mark are non-significant. π-A isotherms of **M)**
650 DLPC (12:0), DMPC (14:0), DPPC (16:0) and DSPC (18:0) with and without bacterial
651 MVs obtained at 25°C**. N)** Variability in compressibility modulus plotted as a function of
652 surface pressure acquired for DLPC (12:0), DMPC (14:0), DPPC (16:0) and DSPC (18:0).
653 **O)** Variation of excess Gibb's free energy of mixing of bacterial MVs with lipid monolayer
654 as a function of increasing surface pressures 0 mN/m, 5 mN/m, 10 mN/m, 15 mN/m and
655 20 mN/m. **P)** Bending force (ΔF_b) histogram of DOPC, DOPG, and PI monolayers at the
656 interface in presence of bacterial MVs. All isotherms were recorded with constant barrier
657 compression speed of 8 mm/min at 25°C. All representative isotherms are the mean of
658 independently performed experiments conducted thrice. For isotherms and compressibility
659 modulus curves the estimated standard error for data points of surface pressure (π) with
660 respect to area per molecule (A) was approximately ±0.05 mN/m.

661 We then sought to question the role of lipid acyl chain length in MV interaction/fusion
662 using monolayer of lipids at the air-water interface. This is important as under cellular
663 conditions transient phase separated regions might differ in the membrane thickness [28].
664 Analysis of surface pressure-area curves of monolayers of increasing acyl chain length,
665 which corresponds to membrane bilayer thickness, were in good agreement with previous
666 reports [29]. We observed that the mean molecular area occupied by phospholipids decrease
667 with increasing chain length in control conditions i.e. in absence of bacterial MVs, except
668 DPPC (***Fig. 4M***), which can be explained by the effective acyl chain hydrophobic
669 interactions[30]. In presence of bacterial MVs, increase in area per molecule was observed in

670 each of the four membrane monolayers with rise in surface pressure (***Fig. 4M***). The
671 observed increase in molecular area was fairly constant throughout all the phases in DLPC,
672 DPPC and DSPC membrane monolayers (***Fig. 4M***) whereas an increasing trend was
673 observed in DMPC till 15 mN/m (***Fig. 4M***). Decrease in collapse pressure by 3.15 mN/m
674 and 5.04 mN/m was calculated for DLPC and DMPC. Highest decrease in collapse pressure
675 of ~ -7 mN/m amongst all lipids was observed for DPPC after MV addition suggests most
676 significant bending of membrane in 16:0 acyl chain length (***Fig 4P***). This decline was least
677 in case of DSPC (***Fig. 4P***). ***Fig. 4N*** show monolayer compressibility curves of the lipids
678 in presence of MV with respect to control. A decline in compressibility modulus by around
679 10 mN/m was seen in DLPC (***Fig 4N***), whereas a decline of 35 mN/m was observed in
680 DPPC (***Fig. 4N***). Compressibility modulus showed a dramatic increase in case of DMPC
681 and DSPC with a value of almost 50 mN/m and 60 mN/m (***Fig. 4N***) and lowest energy
682 change of mixing was observed in case of DMPC throughout all pressures (***Fig. 6O and***
683 ***Table S3***). The ΔG_{Excess} change though followed falling trend up to a particular pressure,
684 there was not much difference between the Gibb's free energy curves of varying acyl chain
685 length containing lipids (***Fig. 6O***). At 15 mN/m, the free energy change was highest in
686 DLPC followed by DPPC suggesting ideal mixing of bacterial MVs with these membranes.

687 **Lipid membrane rigidity and phase separation modulate OMV fusion**

688 Host cell membranes are multi-component lipid assembly that is a non-equilibrium
689 homogenous system close to phase separation. The membrane environment has highly
690 transient phase separating regions called rafts important for cellular signaling. We therefore
691 investigated the effect of phase behavior on the interaction of the bacterial MVs. In order
692 to probe this, we reconstituted liposomes (GUVs and LUVs) made of widely accepted
693 ternary membrane composition (i.e., DOPC:BSM:Cholesterol) and varied the amounts of
694 cholesterol to enable different degrees of liquid-disordered (L_d) and liquid-ordered (L_o)
695 regions. This would mimic the biologically relevant highly dynamic local changes in
696 membrane phase boundaries [31]. First, we reconstituted GUVs composed of DOPC/BSM
697 without any cholesterol representing a disordered (L_d) phase in membrane to examine how
698 the L_d forming membrane condition effects the interaction of MV (*liquid disordered;*
699 *DOPC:BSM:Chol 5:5:0*) [32]. Uniform fusion of bacterial MVs to the partial disordered
700 membrane was observed. We arrived at this conclusion by monitoring all the planes of

701 stacks as well as 3D-stack image of GUV incubated with bacterial MVs (***Fig. 5A***). The
702 fluorescence anisotropy of the dye increased by ~ 27% upon interaction with MV in a
703 concentration dependent manner indicating decrease in membrane fluidity (***Fig. 5B***).
704 Further, the membrane dipole potential was found to linearly decrease upon the interaction
705 of MV (***Fig. 5C-5D***), all of which hint at binding of bacterial MVs that may allow some
706 lipid mixing [33].

707 We then modulated the degree of phase separation, which in turn effects the line tension at
708 the phase separating boundaries [34], by reconstituting membranes having L_o/L_d phase
709 separated regions by changing the cholesterol levels (i.e, *DOPC:BSM:Chol, 4:4:2/3:3:4*).
710 Interestingly, in case of L_o/L_d phase separating membranes with moderate levels of
711 cholesterol (*DOPC:BSM:Chol, 4:4:2*) significant binding of bacterial MVs was observed
712 (***Fig. 5E***). The fluidity decreased in a similar manner as for the L_o membrane as reflected
713 in the increase fluorescence anisotropy of the dye by ~15 % (***Fig. 5F***). Similarly, the dipole
714 potential was found to linearly decrease upon the interaction of MV (***Fig. 5G-5H***).
715 Interestingly, in case of phase separating membranes comprising higher amount of
716 cholesterol (*DOPC:BSM:Chol, 3:3:4*), having a larger L_o (liquid ordered) regions the MV
717 binding was found to be relatively weak (***Fig. 5I***). Also, the fluidity was found to decrease
718 as in earlier cases, however, no significant change in the dipole potential of the membrane
719 (***Figs. 5J-5L***).

720 We then investigated the role of cholesterol in bacterial MV interaction/fusion and the
721 subsequent mechano-elastic changes in lipid monolayer. To this end, as described earlier π
722 -*A* isotherms of show similar trend with increase in molecular area in the presence of MV
723 (***Fig. 5M***). A noticeable aspect observed in the monolayer with highest cholesterol content
724 (3:3:4) in the presence of MV, was that - after surface pressure of around 7.5 mN/m, there
725 was a left shift followed by a right shift after 35 mN/m (***Fig. 5O and 5T***). Collapse pressure
726 reduced in both partially disordered DOPC/BSM membrane without any cholesterol and
727 DOPC/BSM/Chol(3:3:4) while increased by ~ 0.5 mN/m in the case of
728 DOPC/BSM/Chol(4:4:2) membrane(***Fig. 5T, and Table S2***).
729

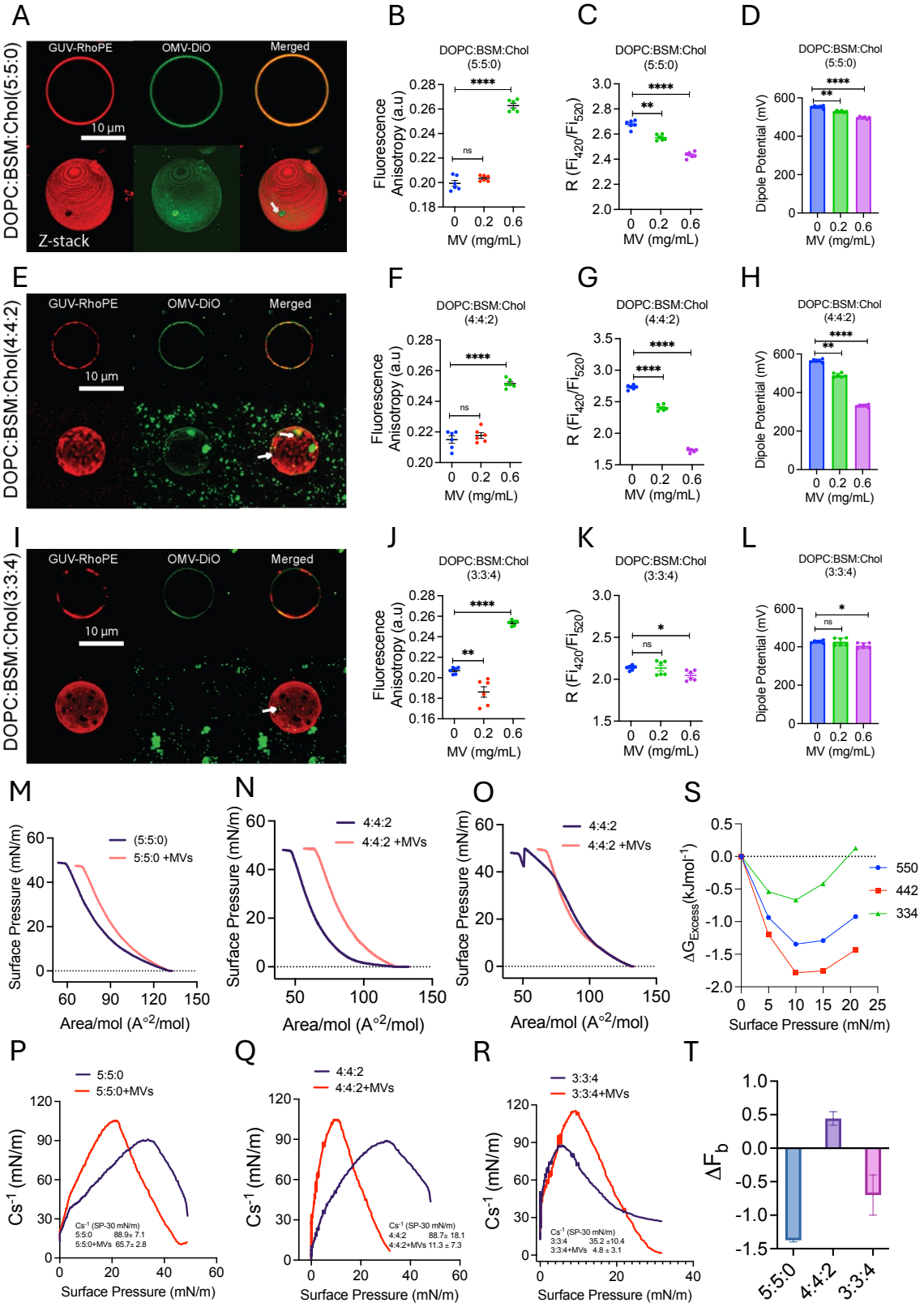
A
B
C
D
E
F
G
H
I
J
K
L
M
N
O
S
P
Q
R
T
DOPC:BSM:Chol(5:5:0)
DOPC:BSM:Chol(4:4:2)
DOPC:BSM:Chol(3:3:4)
GUV-RhoPE
OMV-DiO
Merged
10 µm
Z-stack
Fluorescence Anisotropy (a.u)
R (Fi420/Fi520)
Dipole Potential (mV)
MV (mg/mL)
Surface Pressure (mN/m)
Area/mol (A°2/mol)
ΔGExcess(kJmol-1)
Cs-1 (mN/m)
ΔFb
(5:5:0)
5:5:0 +MVs
4:4:2
4:4:2 +MVs
550
442
334
5:5:0
5:5:0+MVs
4:4:2
4:4:2+MVs
3:3:4
3:3:4+MVs

732 ***Figure 5.*** **Effect of increasing concentration of cholesterol (liquid order) and phase**
733 **behavior of membrane on binding, changes in membrane parameters treated with**
734 **bacterial MVs. A)** Fluorescence image showing GUVs composed of DOPC:BSM:Chol in
735 the molar ratio of 5:5:0 doped with 1 mole % Rhodamine PE (*red channel)* interaction with
736 DiO labelled bacterial MVs *(green channel)*. Bacterial MVs distribution on equatorial
737 plane of GUVs is represented by merged image of both red and green channels along with
738 the 3D stack of each channel. **B)** Fluorescence anisotropy of partially disordered
739 DOPC:BSM:Chol 5:5:0 membrane induced by bacterial MVs, **C and D)** Dipole potential
740 of partially disordered (DOPC:BSM:Chol 5:5:0) treated with increasing concentration of
741 bacterial MVs**. E)** Multiple lipid domain can confine the binding of bacterial MVs to
742 partially disordered DOPC:BSM:Chol 4:4:2 membrane (*left*- Rhodamine PE- (red), *centre*-
743 DiO (green) and *right*- merged). Top panel is showing MV binding to equatorial plane of
744 GUVs and the panel below is bacterial MVs 3D-stack of GUV-MVs mixture. **F)** Membrane
745 fluidity variation in DOPC:BSM:Chol in molar ratio of 4:4:2 membrane treated with
746 bacterial MVs in increasing concentration. **G and H)** Dipole potential of
747 (DOPC:BSM:Chol) in mole ratio of 4:4:2 treated with bacterial MVs in increasing
748 concentration. **I)** Fluorescence image showing GUVs composed of DOPC:BSM:Chol in
749 the molar ratio of 3:3:4 correspond to liquid ordered domain (l_o) doped with 1 mole %
750 Rhodamine PE (*red channel)* interaction with DiO labelled MVs *(green channel)*. bacterial
751 MVs has least binding with DOPC:BSM:Chol; 3:3:4 represented by merged image of both
752 red and green channels along with the 3D stack of each channel. **J)** Changes in anisotropy
753 of DOPC:BSM:Chol (3:3:4) treated with increasing concentration of bacterial MVs. **K and**
754 **L)** Fluorescence ratio and dipole potential of (DOPC:BSM:Chol 3:3:4) treated with
755 increasing concentration of Bacterial MVs. At least 30 GUVS visualized under microscope
756 and scale bar is 10 µm. All fluorescence spectroscopic data are shown as mean ± S.E. from
757 three independent experiments. Significant variations were compared through one-sided
758 ANOVA of membrane condition treated with bacterial MVs with respect to control (only
759 lipid membrane without bacterial MVs), where, (***) depicts $p<0.001$, (**) $p<0.01$ and (*)
760 $p<0.05$, test data point (membrane treated with bacterial MVs) with no asterisk mark are
761 non-significant.

762 π-A isotherms of **M)** 5:5:0 (BSM:DOPC:cholesterol), **N)** 4:4:2 (BSM:DOPC: cholesterol)
763 and **O)** 3:3:4 (BSM:DOPC:cholesterol) with and without bacterial MVs obtained at 25°C.
764 Variability in compressibility modulus plotted as a function of surface pressure acquired
765 for **P)** 5:5:0, **Q)** 4:4:2 and **R)** 3:3:4 from respective Langmuir isotherms. **S)** Variation of
766 excess Gibb's free energy of mixing of bacterial MVs with cholesterol containing
767 membrane as a function of increasing surface pressures 0 mN/m, 5 mN/m, 10 mN/m, 15
768 mN/m and 20 mN/m. **(F)** Bending force (ΔF_b) histogram of 5:5:0, 4:4:2 and 3:3:4
769 monolayers at the interface in presence of bacterial MVs. All isotherms were recorded with
770 constant barrier compression speed of 8 mm/min at 25°C. All representative isotherms are
771 the mean of independently performed experiments conducted thrice. For isotherms and
772 compressibility modulus curves the estimated standard error for data points of surface
773 pressure (π) with respect to area per molecule (A) was approximately ±0.05 mN/m.
774

775 ## Discussion

776 Membrane fusion is considered one of the key mechanisms for the entry of bacterial MVs
777 inside the host cells [2, 15]. Using a non-pathogenic *E. coli* strain as a model Gram-negative
778 bacterium to isolate bacterial MVs, we quantitatively investigate MVs interaction with host
779 membrane to dissect the MV mediated modulation of host membrane fluidity, dipole
780 potential, compressibility parameters that might change as a result of fusion and alter
781 subsequent signalling. Fusion of bacterial MVs to host membranes is involved in
782 transmission of virulence factors in non-phagocytic cells [19] as well as in reprogramming of
783 phagosomes in phagocytic macrophage[35]. As expected, the fluorescently labelled bacterial
784 MVs was found to undergo significant internalization by THP-1 macrophage (***Fig. 1***), in
785 line with previous observations (11). The binding of DiO-labelled and Di-8-ANEPPS-
786 labelled bacterial MVs to the reconstituted lipid membranes mimicking the outer-leaflet of
787 the host cell membrane was found to be homogenous (***Fig. 2***). The enhanced FRET
788 observed upon incubation of probed LUVs with unprobed MVs confirms fusion (***Fig. 2***).
789 Further, observed monolayer area expansion accompanied by an ideal mixing reflected in
790 a negative free energy change might also hint at likely fusion of MV, although adhesion
791 not progressing into complete fusion cannot be totally ruled out. We observe that the fusion

792 of bacterial MVs results in increased fluidization and dipole potential (***Fig. 2***). Further, it
793 also increased the magnitude of the membrane surface potential of the host model
794 membrane to more negative regime. Such trans-negative membrane surface potential was
795 reported to be essential for cell-cell fusion[36]. The observed fluidization is supported by the
796 experimentally determined increase in molecular area per lipid as well as Compressibility
797 (as seen in decrease in the C_s^{-1} at surface pressure at 30 mN/m) (***Fig. 2***). The surface-
798 pressure area isotherm of the lipid fraction of MV devoid of any proteins suggests that the
799 MV membrane is extremely rigid as evident from the low collapse pressure (***Fig. S4***). LPS,
800 the major component of MV owing to its relatively wider cross-section area and low head-
801 to-tail aspect ratio could be a major contributor towards fluidization as it is known to
802 uniformly adhere and incorporate in egg-PC, and DOPE containing lipid bilayer [37] all of
803 which are present in the host outer leaflet of the membrane. This is in line with recent
804 findings that Phthiocerol dimycocerosates (DIMs), a lipid component of *Mycobacterium*
805 *tuberculosis,* are transferred to and accommodated in the host cell membrane due to its
806 conical shape [38].

807 We then wondered how would the acyl chain length effect the fusion? MV fusion to major
808 phospholipid DOPC, DOPG and PI (***Fig. 3***) but not BSM membrane, results in enhanced
809 membrane fluidity as well as increased dipole potential (***Fig S4***). The changes in area per
810 lipid molecule are coupled to the degree of interfacial fusion of the interacting components
811 [23, 39]. The observed increase in area per lipid molecule is likely due to the formation of
812 inverted cubic structure/aggregates at the fusion sites resulting in expulsion of some lipids
813 [37, 38, 40], which, also explains the observed relatively higher negative values of G_{Excess} . We
814 observed that DLPC, DMPC, and DSPC membranes exhibited increased rigidity. This
815 rigidity could be attributed to partial fusion occurring within the bilayers, resulting in a
816 shift towards the native ordered phase of the bilayers. Interestingly, we observed that MV
817 fusion to only DPPC membrane results in enhanced fluidization accompanied by increase
818 in interfacial molecular dipoles unlike other lipid membrane (***Fig. 4C***). Together, the data
819 suggest that while MV interaction is facilitated by zwitterionic head groups, however, an
820 optimum acyl chain length is essential for effective interaction/fusion in line with previous

821 observations [41].

822 Lipid rafts have been reported to facilitate the fusion of bacterial MVs [8]. However, this was
823 proved using cholesterol depleting or sequestering agents such as filipin or Methyl-ß-
824 cyclodextrin, which cannot rule out the possibility that disruption of cholesterol on a large
825 scale may affect protein dependent processes not limited to lipid rafts. One way to examine
826 and correlate the exclusive dependence of MV mixing with lipid rafts is by reconstituting
827 minimal systems of lipid raft-like regions without any protein. Bacterial MVs were found
828 to show strongest fusion to partially disordered membranes devoid of cholesterol
829 (DOPC:BSM:Chol, 5:5:0) accompanied by highest decrease in the fluidity (***Fig. 5***).
830 Further, increase in the cholesterol in the membrane lead to decreased fusion of bacterial
831 MVs to the membrane (***Fig. 5).*** The increasing cholesterol levels results in co-existing
832 phase separated regions (L_o and L_d) within the membranes (DOPC:BSM:Chol, 4:4:2 &
833 3:3:4), however, the number of the phase separating boundaries is higher in the former.
834 Such differences in the phase separating boundaries would accumulate different degrees of
835 interfacial energy in the membrane, that would facilitate the fusion of bacterial MVs in
836 different ways, which explains the observed variation [20, 42].

837 Increase in the dipole potential of host lipid membrane by fusion of MV is likely to
838 stimulate conformational changes in the membrane bound/inserted receptor proteins [20, 34].
839 Such conformational changes in transmembrane receptor proteins have been reported to
840 significantly alter the receptor signaling in host cells [43]. Additionally, our study also
841 suggests that MV interaction with lipid rafts/phase boundaries may have an important role
842 in altering host cell signaling [44]. *Mycobacterium ulcerans* endotoxin, Mycolactone, was
843 shown to have potent effect on reorganization of raft-like model membranes [45]. Although
844 our observations are based on a non-pathogenic strain of *E. coli* as a model bacteria, it is
845 important to note that similar observations can be expected with pathogenic *E. coIi* as they
846 share more than 70% similarity in the protein content of the their membrane vesicles [46].
847 Besides the overall changes induced by the MVs, identifying the potential proteins in the
848 MVs and their contribution to the modulation of the host cell membrane remains an
849 important aspect that would require extensive research.

850

851 ## Author Contributions

852 AP and MS conceived the idea and designed the research. AP, AT carried out the
853 characterization of bacterial MVs. DKS helped with MV characterization. AP, DK and GM
854 performed labelling of bacterial MVs and imaging experiments. AP and TM performed
855 monolayer experiments. AP and GM performed fluorimetry experiments. AP, AT, TM,
856 GM and MS analyzed the data. AP, TM and MS wrote the manuscript.

857 ## Acknowledgements

858 We would like to gratefully acknowledge the financial support received from the
859 Department of Science and Technology (EMR/2017/004513) and Department of
860 Biotechnology, Govt. of India (BT/PR/21226/MED/122/41/2016). AP, AT and TM
861 acknowledge MHRD for the GATE fellowship. We would also like to thank Department
862 of Atomic Energy, Govt. of India and NISER, Bhubaneshwar for financial support and
863 infrastructure.

864 ## Conflict of Interests

865 Authors declare no competing interests.

866 ## References

867 (1) Beveridge, T. J. Structures of gram-negative cell walls and their derived membrane
868 vesicles. *Journal of bacteriology* **1999**, *181* (16), 4725-4733. Schwechheimer, C.; Kuehn,
869 M. J. Outer-membrane vesicles from Gram-negative bacteria: biogenesis and functions.
870 *Nature Reviews Microbiology* **2015**, *13* (10), 605.
871 (2) Kulp, A.; Kuehn, M. J. Biological functions and biogenesis of secreted bacterial outer
872 membrane vesicles. *Annual review of microbiology* **2010**, *64*, 163-184.
873 (3) Toyofuku, M.; Nomura, N.; Eberl, L. Types and origins of bacterial membrane vesicles.
874 *Nature Reviews Microbiology* **2018**, 1. Théry, C.; Witwer, K. W.; Aikawa, E.; Alcaraz, M.
875 J.; Anderson, J. D.; Andriantsitohaina, R.; Antoniou, A.; Arab, T.; Archer, F.; Atkin-Smith,
876 G. K. Minimal information for studies of extracellular vesicles 2018 (MISEV2018): a
877 position statement of the International Society for Extracellular Vesicles and update of the
878 MISEV2014 guidelines. *Journal of extracellular vesicles* **2018**, *7* (1), 1535750.
879 (4) Koeppen, K.; Hampton, T. H.; Jarek, M.; Scharfe, M.; Gerber, S. A.; Mielcarz, D. W.;
880 Demers, E. G.; Dolben, E. L.; Hammond, J. H.; Hogan, D. A. A novel mechanism of host-
881 pathogen interaction through sRNA in bacterial outer membrane vesicles. *PLoS pathogens*
882 **2016**, *12* (6), e1005672.
883 (5) MacDonald, I. A.; Kuehn, M. J. Offense and defense: microbial membrane vesicles
884 play both ways. *Research in microbiology* **2012**, *163* (9-10), 607-618.
885 (6) Chattopadhyay, M. K.; Jagannadham, M. V. Vesicles-mediated resistance to antibiotics
886 in bacteria. *Frontiers in microbiology* **2015**, *6*, 758.
887 (7) Kaparakis-Liaskos, M.; Ferrero, R. L. Immune modulation by bacterial outer membrane
888 vesicles. *Nature reviews Immunology* **2015**, *15* (6), 375.
889 (8) Bomberger, J. M.; MacEachran, D. P.; Coutermarsh, B. A.; Ye, S.; O'Toole, G. A.;
890 Stanton, B. A. Long-distance delivery of bacterial virulence factors by Pseudomonas
891 aeruginosa outer membrane vesicles. *PLoS pathogens* **2009**, *5* (4), e1000382.
892 (9) Jäger, J.; Keese, S.; Roessle, M.; Steinert, M.; Schromm, A. B. Fusion of L egionella
893 pneumophila outer membrane vesicles with eukaryotic membrane systems is a mechanism
894 to deliver pathogen factors to host cell membranes. *Cellular microbiology* **2015**, *17* (5),
895 607-620.

896 (10) Sezgin, E.; Kaiser, H.-J.; Baumgart, T.; Schwille, P.; Simons, K.; Levental, I.
897 Elucidating membrane structure and protein behavior using giant plasma membrane
898 vesicles. *nature protocols* **2012**, *7* (6), 1042.
899 (11) Folch, J.; Lees, M.; Sloane Stanley, G. A simple method for the isolation and
900 purification of total lipides from animal tissues. *J biol Chem* **1957**, *226* (1), 497-509. Reis,
901 A.; Rudnitskaya, A.; Blackburn, G. J.; Fauzi, N. M.; Pitt, A. R.; Spickett, C. M. A
902 comparison of five lipid extraction solvent systems for lipidomic studies of human LDL.
903 *Journal of lipid research* **2013**, *54* (7), 1812-1824.
904 (12) Weinberger, A.; Tsai, F.-C.; Koenderink, G. H.; Schmidt, T. F.; Itri, R.; Meier, W.;
905 Schmatko, T.; Schröder, A.; Marques, C. Gel-assisted formation of giant unilamellar
906 vesicles. *Biophysical journal* **2013**, *105* (1), 154-164.
907 (13) Starke-Peterkovic, T.; Turner, N.; Vitha, M. F.; Waller, M. P.; Hibbs, D. E.; Clarke,
908 R. J. Cholesterol effect on the dipole potential of lipid membranes. *Biophysical journal*
909 **2006**, *90* (11), 4060-4070.
910 (14) Mondal, S.; Sarkar, M. Non-steroidal anti-inflammatory drug induced membrane
911 fusion: concentration and temperature effects. *The Journal of Physical Chemistry B* **2009**,
912 *113* (51), 16323-16331. Struck, D. K.; Hoekstra, D.; Pagano, R. E. Use of resonance energy
913 transfer to monitor membrane fusion. *Biochemistry* **1981**, *20* (14), 4093-4099.
914 (15) O'donoghue, E. J.; Krachler, A. M. Mechanisms of outer membrane vesicle entry into
915 host cells. *Cellular microbiology* **2016**, *18* (11), 1508-1517.
916 (16) Greenspan, P.; Mayer, E. P.; Fowler, S. D. Nile red: a selective fluorescent stain for
917 intracellular lipid droplets. *The Journal of cell biology* **1985**, *100* (3), 965-973.
918 (17) Wang, X.; Eagen, W. J.; Lee, J. C. Orchestration of human macrophage NLRP3
919 inflammasome activation by Staphylococcus aureus extracellular vesicles. *Proceedings of*
920 *the National Academy of Sciences* **2020**.
921 (18) Van Meer, G.; Voelker, D. R.; Feigenson, G. W. Membrane lipids: where they are and
922 how they behave. *Nature reviews Molecular cell biology* **2008**, *9* (2), 112. Ingólfsson, H.
923 I.; Carpenter, T. S.; Bhatia, H.; Bremer, P.-T.; Marrink, S. J.; Lightstone, F. C.
924 Computational lipidomics of the neuronal plasma membrane. *Biophysical journal* **2017**,
925 *113* (10), 2271-2280.

926 (19) O'Donoghue, E. J.; Sirisaengtaksin, N.; Browning, D. F.; Bielska, E.; Hadis, M.;
927 Fernandez-Trillo, F.; Alderwick, L.; Jabbari, S.; Krachler, A. M. Lipopolysaccharide
928 structure impacts the entry kinetics of bacterial outer membrane vesicles into host cells.
929 *PLoS pathogens* **2017**, *13* (11), e1006760.
930 (20) Yang, S.-T.; Kiessling, V.; Tamm, L. K. Line tension at lipid phase boundaries as
931 driving force for HIV fusion peptide-mediated fusion. *Nature communications* **2016**, *7*,
932 11401.
933 (21) Bandari, S.; Chakraborty, H.; Covey, D. F.; Chattopadhyay, A. Membrane dipole
934 potential is sensitive to cholesterol stereospecificity: implications for receptor function.
935 *Chemistry and physics of lipids* **2014**, *184*, 25-29.
936 (22) Gross, E.; Bedlack Jr, R. S.; Loew, L. M. Dual-wavelength ratiometric fluorescence
937 measurement of the membrane dipole potential. *Biophysical journal* **1994**, *67* (1), 208-216.
938 (23) Brockman, H. Lipid monolayers: why use half a membrane to characterize protein-
939 membrane interactions? *Current opinion in structural biology* **1999**, *9* (4), 438-443.
940 (24) Allende, D.; Vidal, A.; McIntosh, T. J. Jumping to rafts: gatekeeper role of bilayer
941 elasticity. *Trends in biochemical sciences* **2004**, *29* (6), 325-330. Brown, R. E.; Brockman,
942 H. L. Using monomolecular films to characterize lipid lateral interactions. In *Lipid Rafts*,
943 Springer, 2007; pp 41-58. Smaby, J. M.; Kulkarni, V. S.; Momsen, M.; Brown, R. E. The
944 interfacial elastic packing interactions of galactosylceramides, sphingomyelins, and
945 phosphatidylcholines. *Biophysical journal* **1996**, *70* (2), 868-877.
946 (25) Feng, S.-s. Interpretation of mechanochemical properties of lipid bilayer vesicles from
947 the equation of state or pressure− area measurement of the monolayer at the air− water or
948 oil− water interface. *Langmuir* **1999**, *15* (4), 998-1010. Pinto, O. A.; Disalvo, E. A. A new
949 model for lipid monolayer and bilayers based on thermodynamics of irreversible processes.
950 *Plos one* **2019**, *14* (4), e0212269. Auerswald, A.; Gruber, T.; Balbach, J.; Meister, A. Lipid-
951 Dependent Interaction of Human N-BAR Domain Proteins with Sarcolemma Mono-and
952 Bilayers. *Langmuir* **2020**, *36* (30), 8695-8704.
953 (26) Goodrich, F. Proceedings, 2nd International Congress on Surface Activity. *Vol. I* **1957**,
954 85.

955 (27) Peetla, C.; Jin, S.; Weimer, J.; Elegbede, A.; Labhasetwar, V. Biomechanics and
956 thermodynamics of nanoparticle interactions with plasma and endosomal membrane lipids
957 in cellular uptake and endosomal escape. *Langmuir* **2014**, *30* (25), 7522-7532.
958 (28) Lewis, B. A.; Engelman, D. M. Lipid bilayer thickness varies linearly with acyl chain
959 length in fluid phosphatidylcholine vesicles. *Journal of molecular biology* **1983**, *166* (2),
960 211-217.
961 (29) Miyoshi, T.; Kato, S. Detailed analysis of the surface area and elasticity in the
962 saturated 1, 2-diacylphosphatidylcholine/cholesterol binary monolayer system. *Langmuir*
963 **2015**, *31* (33), 9086-9096.
964 (30) Zhao, L.; Feng, S.-S. Effects of lipid chain length on molecular interactions between
965 paclitaxel and phospholipid within model biomembranes. *Journal of colloid and interface*
966 *science* **2004**, *274* (1), 55-68.
967 (31) Simons, K.; Ikonen, E. Functional rafts in cell membranes. *nature* **1997**, *387* (6633),
968 569.
969 (32) Yang, S.-T.; Kiessling, V.; Simmons, J. A.; White, J. M.; Tamm, L. K. HIV gp41–
970 mediated membrane fusion occurs at edges of cholesterol-rich lipid domains. *Nature*
971 *chemical biology* **2015**, *11* (6), 424.
972 (33) Ermakov, Y. A.; Averbakh, A. Z.; Yusipovich, A. I.; Sukharev, S. Dipole potentials
973 indicate restructuring of the membrane interface induced by gadolinium and beryllium
974 ions. *Biophysical journal* **2001**, *80* (4), 1851-1862.
975 (34) Chen, D.; Santore, M. M. Large effect of membrane tension on the fluid–solid phase
976 transitions of two-component phosphatidylcholine vesicles. *Proceedings of the National*
977 *Academy of Sciences* **2014**, *111* (1), 179-184.
978 (35) Ge, J.; Shao, F. Manipulation of host vesicular trafficking and innate immune defence
979 by Legionella Dot/Icm effectors. *Cellular microbiology* **2011**, *13* (12), 1870-1880. Hubber,
980 A.; Roy, C. R. Modulation of host cell function by Legionella pneumophila type IV
981 effectors. *Annual review of cell and developmental biology* **2010**, *26*, 261-283.
982 (36) Asawakarn, T.; Cladera, J.; O'Shea, P. Effects of the membrane dipole potential on
983 the interaction of saquinavir with phospholipid membranes and plasma membrane
984 receptors of Caco-2 cells. *Journal of Biological Chemistry* **2001**, *276* (42), 38457-38463.
985 Samsonov, A. V.; Chatterjee, P. K.; Razinkov, V. I.; Eng, C. H.; Kielian, M.; Cohen, F. S.

986 Effects of membrane potential and sphingolipid structures on fusion of Semliki Forest
987 virus. *Journal of virology* **2002**, *76* (24), 12691-12702. Wang, L.; Bose, P. S.; Sigworth, F.
988 J. Using cryo-EM to measure the dipole potential of a lipid membrane. *Proceedings of the*
989 *National Academy of Sciences* **2006**, *103* (49), 18528-18533.
990 (37) Nomura, K.; Inaba, T.; Morigaki, K.; Brandenburg, K.; Seydel, U.; Kusumoto, S.
991 Interaction of lipopolysaccharide and phospholipid in mixed membranes: solid-state 31P-
992 NMR spectroscopic and microscopic investigations. *Biophysical journal* **2008**, *95* (3),
993 1226-1238.
994 (38) Augenstreich, J.; Haanappel, E.; Ferré, G.; Czaplicki, G.; Jolibois, F.; Destainville, N.;
995 Guilhot, C.; Milon, A.; Astarie-Dequeker, C.; Chavent, M. The conical shape of DIM lipids
996 promotes Mycobacterium tuberculosis infection of macrophages. *Proceedings of the*
997 *National Academy of Sciences* **2019**, *116* (51), 25649-25658.
998 (39) Mura, M.; Dennison, S. R.; Zvelindovsky, A. V.; Phoenix, D. A. Aurein 2.3
999 functionality is supported by oblique orientated α-helical formation. *Biochimica et*
1000 *Biophysica Acta (BBA)-Biomembranes* **2013**, *1828* (2), 586-594.
1001 (40) Adams, P. G.; Lamoureux, L.; Swingle, K. L.; Mukundan, H.; Montaño, G. A.
1002 Lipopolysaccharide-induced dynamic lipid membrane reorganization: tubules,
1003 perforations, and stacks. *Biophysical journal* **2014**, *106* (11), 2395-2407.
1004 (41) Szule, J. A.; Fuller, N. L.; Rand, R. P. The effects of acyl chain length and saturation
1005 of diacylglycerols and phosphatidylcholines on membrane monolayer curvature.
1006 *Biophysical journal* **2002**, *83* (2), 977-984.
1007 (42) Risselada, H. J.; Marelli, G.; Fuhrmans, M.; Smirnova, Y. G.; Grubmüller, H.;
1008 Marrink, S. J.; Müller, M. Line-tension controlled mechanism for influenza fusion. *PLoS*
1009 *One* **2012**, *7* (6), e38302.
1010 (43) Zhou, Y.; Wong, C.-O.; Cho, K.-j.; Van Der Hoeven, D.; Liang, H.; Thakur, D. P.;
1011 Luo, J.; Babic, M.; Zinsmaier, K. E.; Zhu, M. X. Membrane potential modulates plasma
1012 membrane phospholipid dynamics and K-Ras signaling. *Science* **2015**, *349* (6250), 873-
1013 876.
1014 (44) Kovács, T.; Batta, G.; Hajdu, T.; Szabó, Á.; Váradi, T.; Zákány, F.; Csomós, I.;
1015 Szöllősi, J.; Nagy, P. The dipole potential modifies the clustering and ligand binding
1016 affinity of ErbB proteins and their signaling efficiency. *Scientific reports* **2016**, *6*, 35850.

1017 (45) Nitenberg, M.; Benarouche, A.; Maniti, O.; Marion, E.; Marsollier, L.; Géan, J.;
1018 Dufourc, E. J.; Cavalier, J.-F.; Canaan, S.; Girard-Egrot, A. P. The potent effect of
1019 mycolactone on lipid membranes. *PLoS pathogens* **2018**, *14* (1), e1006814.
1020 (46) Lee, E. Y.; Bang, J. Y.; Park, G. W.; Choi, D. S.; Kang, J. S.; Kim, H. J.; Park, K. S.;
1021 Lee, J. O.; Kim, Y. K.; Kwon, K. H. Global proteomic profiling of native outer membrane
1022 vesicles derived from Escherichia coli. *Proteomics* **2007**, *7* (17), 3143-3153. Scorza, F. B.;
1023 Doro, F.; Rodríguez-Ortega, M. J.; Stella, M.; Liberatori, S.; Taddei, A. R.; Serino, L.;
1024 Moriel, D. G.; Nesta, B.; Fontana, M. R. Proteomic characterization of outer membrane
1025 vesicles from the extraintestinal pathogenic Escherichia coli tolR IHE3034 mutant.
1026 *Molecular & Cellular Proteomics* **2007**.
1027

1028

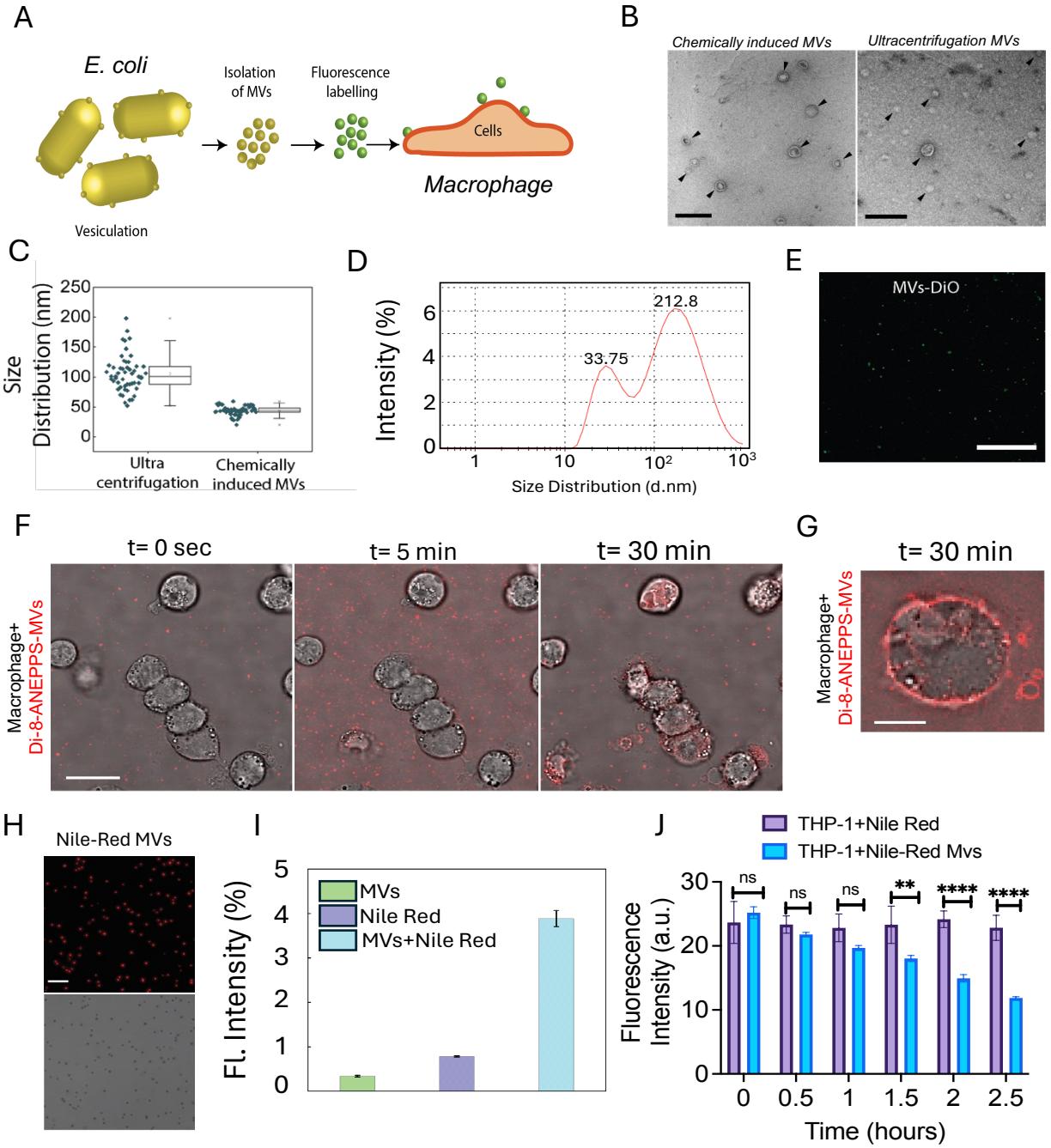
A
E. coli
Isolation of MVs
Fluorescence labelling
Cells
Macrophage
Vesiculation
B
Chemically induced MVs
Ultracentrifugation MVs
C
Size Distribution (nm)
250
200
150
100
50
0
Ultra centrifugation
Chemically induced MVs
D
Intensity (%)
212.8
33.75
Size Distribution (d.nm)
E
MVs-DiO
F
t= 0 sec
t= 5 min
t= 30 min
Macrophage+ Di-8-ANEPPS-MVs
G
t= 30 min
Macrophage+ Di-8-ANEPPS-MVs
H
Nile-Red MVs
I
Fl. Intensity (%)
MVs
Nile Red
MVs+Nile Red
J
THP-1+Nile Red
THP-1+Nile-Red Mvs
Fluorescence Intensity (a.u.)
ns
ns
ns
**
****
****
Time (hours)

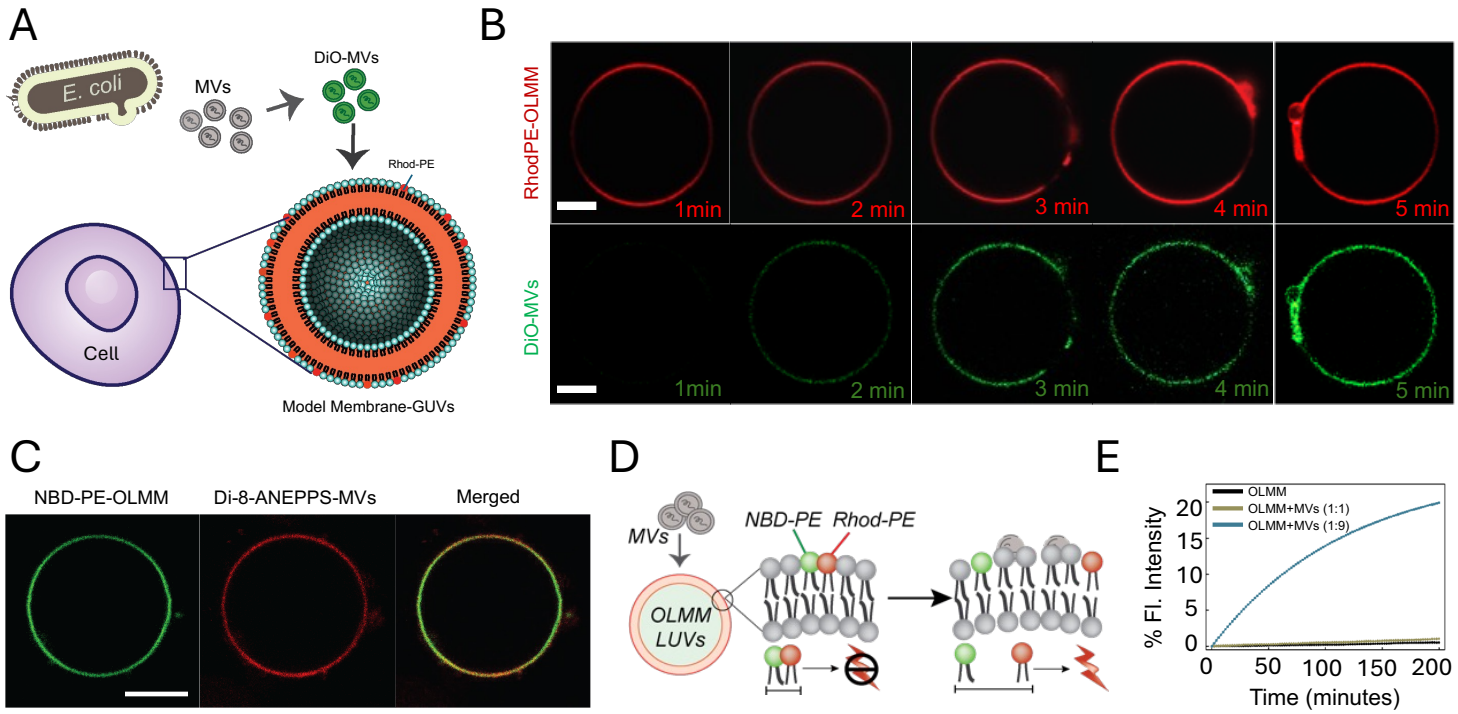
A
E. coli
MVs
DiO-MVs
Rhod-PE
Cell
Model Membrane-GUVs
B
RhodPE-OLMM
DiO-MVs
1min
2 min
3 min
4 min
5 min
C
NBD-PE-OLMM
Di-8-ANEPPS-MVs
Merged
D
MVs
NBD-PE
Rhod-PE
OLMM LUVs
E
OLMM
OLMM+MVs (1:1)
OLMM+MVs (1:9)
% Fl. Intensity
Time (minutes)

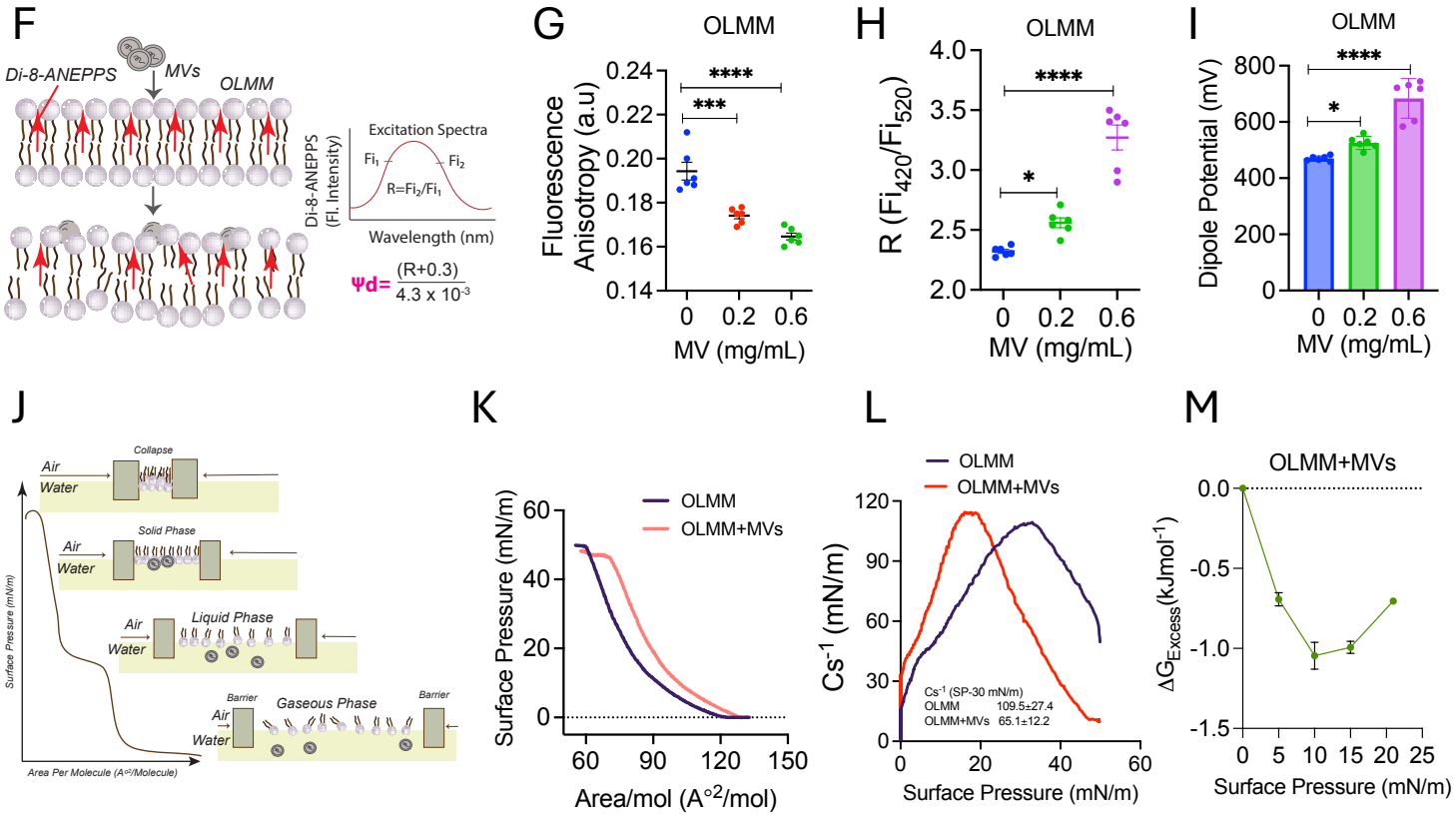
F
Di-8-ANEPPS
MVs
OLMM
Excitation Spectra
Di-8-ANEPPS (Fl. Intensity)
Wavelength (nm)
R=Fi2/Fi1
Ψd= (R+0.3) / 4.3 x 10-3
G
OLMM
Fluorescence Anisotropy (a.u)
MV (mg/mL)
H
OLMM
R (Fi420/Fi520)
MV (mg/mL)
I
OLMM
Dipole Potential (mV)
MV (mg/mL)
J
Air
Water
Collapse
Solid Phase
Liquid Phase
Gaseous Phase
Barrier
Surface Pressure (mN/m)
Area Per Molecule (A°2/Molecule)
K
OLMM
OLMM+MVs
Surface Pressure (mN/m)
Area/mol (A°2/mol)
L
OLMM
OLMM+MVs
Cs-1 (mN/m)
Cs-1 (SP-30 mN/m)
OLMM 109.5±27.4
OLMM+MVs 65.1±12.2
Surface Pressure (mN/m)
M
OLMM+MVs
ΔGExcess(kJmol-1)
Surface Pressure (mN/m)

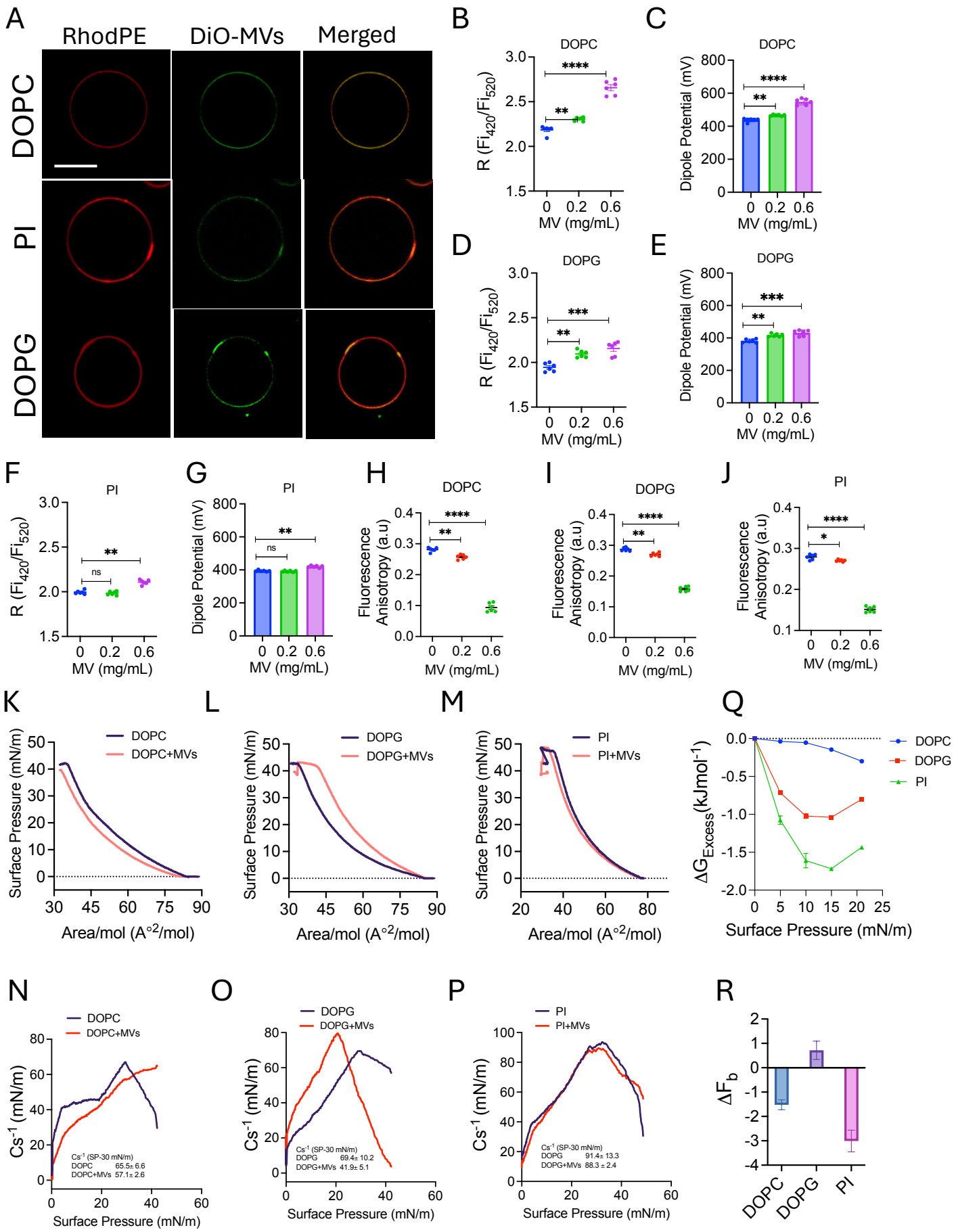
A
RhodPE
DiO-MVs
Merged
DOPC
PI
DOPG
B
DOPC
R (Fi420/Fi520)
MV (mg/mL)
C
DOPC
Dipole Potential (mV)
MV (mg/mL)
D
DOPG
R (Fi420/Fi520)
MV (mg/mL)
E
DOPG
Dipole Potential (mV)
MV (mg/mL)
F
PI
R (Fi420/Fi520)
MV (mg/mL)
G
PI
Dipole Potential (mV)
MV (mg/mL)
H
DOPC
Fluorescence Anisotropy (a.u)
MV (mg/mL)
I
DOPG
Fluorescence Anisotropy (a.u)
MV (mg/mL)
J
PI
Fluorescence Anisotropy (a.u)
MV (mg/mL)
K
DOPC
DOPC+MVs
Surface Pressure (mN/m)
Area/mol (A°2/mol)
L
DOPG
DOPG+MVs
Surface Pressure (mN/m)
Area/mol (A°2/mol)
M
PI
PI+MVs
Surface Pressure (mN/m)
Area/mol (A°2/mol)
Q
DOPC
DOPG
PI
ΔGExcess(kJmol-1)
Surface Pressure (mN/m)
N
DOPC
DOPC+MVs
Cs-1 (mN/m)
Cs-1 (SP-30 mN/m)
DOPC 65.5± 6.6
DOPC+MVs 57.1± 2.6
Surface Pressure (mN/m)
O
DOPG
DOPG+MVs
Cs-1 (mN/m)
Cs-1 (SP-30 mN/m)
DOPG 69.4± 10.2
DOPG+MVs 41.9± 5.1
Surface Pressure (mN/m)
P
PI
PI+MVs
Cs-1 (mN/m)
Cs-1 (SP-30 mN/m)
DOPG 91.4± 13.3
DOPG+MVs 88.3 ± 2.4
Surface Pressure (mN/m)
R
ΔFb
DOPC
DOPG
PI

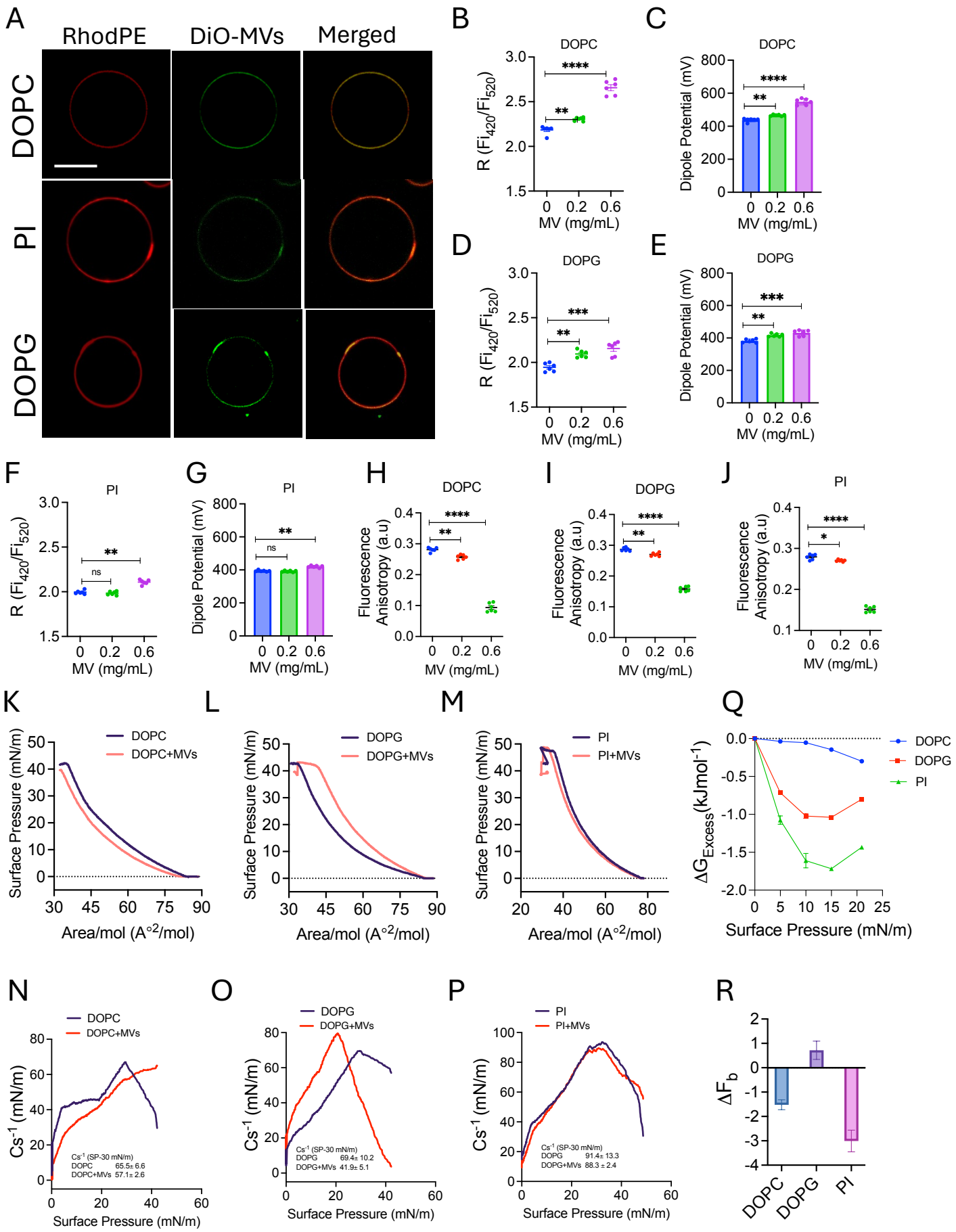
A
RhodPE
DiO-MVs
Merged
DOPC
PI
DOPG
B
DOPC
R (Fi420/Fi520)
MV (mg/mL)
C
DOPC
Dipole Potential (mV)
MV (mg/mL)
D
DOPG
R (Fi420/Fi520)
MV (mg/mL)
E
DOPG
Dipole Potential (mV)
MV (mg/mL)
F
PI
R (Fi420/Fi520)
MV (mg/mL)
G
PI
Dipole Potential (mV)
MV (mg/mL)
H
DOPC
Fluorescence Anisotropy (a.u)
MV (mg/mL)
I
DOPG
Fluorescence Anisotropy (a.u)
MV (mg/mL)
J
PI
Fluorescence Anisotropy (a.u)
MV (mg/mL)
K
DOPC
DOPC+MVs
Surface Pressure (mN/m)
Area/mol (A°2/mol)
L
DOPG
DOPG+MVs
Surface Pressure (mN/m)
Area/mol (A°2/mol)
M
PI
PI+MVs
Surface Pressure (mN/m)
Area/mol (A°2/mol)
Q
DOPC
DOPG
PI
ΔGExcess(kJmol-1)
Surface Pressure (mN/m)
N
DOPC
DOPC+MVs
Cs-1 (mN/m)
Cs-1 (SP-30 mN/m)
DOPC 65.5± 6.6
DOPC+MVs 57.1± 2.6
Surface Pressure (mN/m)
O
DOPG
DOPG+MVs
Cs-1 (mN/m)
Cs-1 (SP-30 mN/m)
DOPG 69.4± 10.2
DOPG+MVs 41.9± 5.1
Surface Pressure (mN/m)
P
PI
PI+MVs
Cs-1 (mN/m)
Cs-1 (SP-30 mN/m)
DOPG 91.4± 13.3
DOPG+MVs 88.3 ± 2.4
Surface Pressure (mN/m)
R
ΔFb
DOPC
DOPG
PI

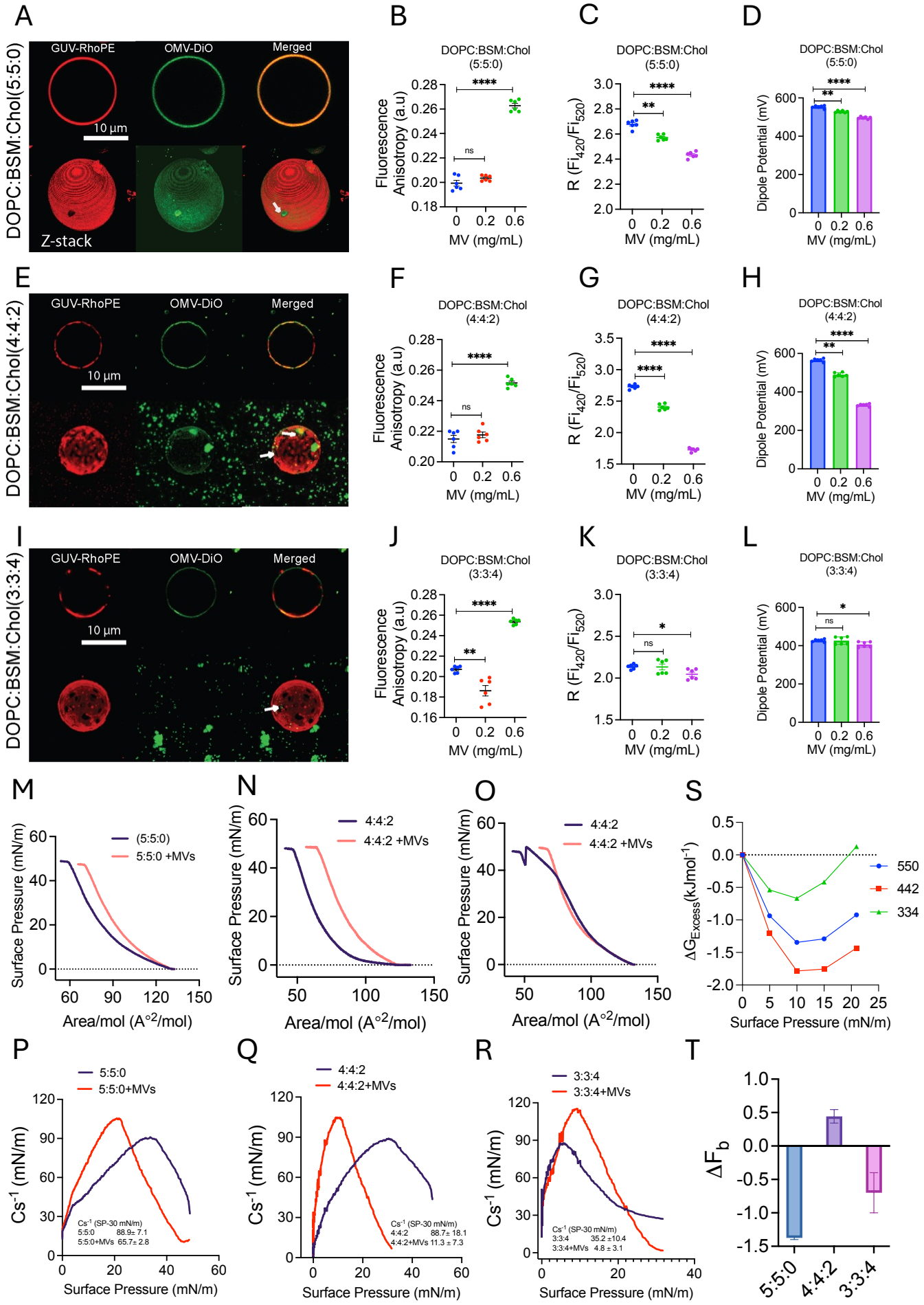
A
DOPC:BSM:Chol(5:5:0)
GUV-RhoPE
OMV-DiO
Merged
10 µm
Z-stack
B
DOPC:BSM:Chol (5:5:0)
Fluorescence Anisotropy (a.u)
MV (mg/mL)
C
DOPC:BSM:Chol (5:5:0)
R (Fi420/Fi520)
MV (mg/mL)
D
DOPC:BSM:Chol (5:5:0)
Dipole Potential (mV)
MV (mg/mL)
E
DOPC:BSM:Chol(4:4:2)
F
DOPC:BSM:Chol (4:4:2)
G
DOPC:BSM:Chol (4:4:2)
H
DOPC:BSM:Chol (4:4:2)
I
DOPC:BSM:Chol(3:3:4)
J
DOPC:BSM:Chol (3:3:4)
K
DOPC:BSM:Chol (3:3:4)
L
DOPC:BSM:Chol (3:3:4)
M
Surface Pressure (mN/m)
Area/mol (A°2/mol)
(5:5:0)
5:5:0 +MVs
N
4:4:2
4:4:2 +MVs
O
4:4:2
4:4:2 +MVs
S
ΔGExcess(kJmol-1)
Surface Pressure (mN/m)
550
442
334
P
5:5:0
5:5:0+MVs
Cs-1 (mN/m)
Surface Pressure (mN/m)
Q
4:4:2
4:4:2+MVs
R
3:3:4
3:3:4+MVs
T
ΔFb
5:5:0
4:4:2
3:3:4